

Cosmological parameters σ_8 , the baryon density Ω_b , and the UV background intensity from a calibrated measurement of H I Lyman α absorption at $z = 1.9$ ¹

David Tytler², David Kirkman, John M. O’Meara, Nao Suzuki, Adam Orin, Dan Lubin, Pascal Paschos, Tridivesh Jena, Wen-Ching Lin, & Michael L. Norman

Center for Astrophysics and Space Sciences;
University of California, San Diego;
MS 0424; La Jolla; CA 92093-0424

ABSTRACT

We identify a concordant model for the intergalactic medium (IGM) at redshift $z = 1.9$ that uses popular values for cosmological and astrophysical parameters and accounts for all baryons with an uncertainty of 6%. The amount of absorption by H I in the IGM provides the best evidence on the physical conditions in the IGM, especially the combination of the mean gas density, the density fluctuations, the intensity of the ionizing flux, and the level of ionization. We have measured the amount of absorption, known as the flux decrement, DA, in the Ly α forest at redshift 1.9. We used spectra of 77 QSO that we obtained with 250 km s⁻¹ resolution from the Kast spectrograph on the Lick observatory 3m telescope. We fit the unabsorbed continua to these spectra using b-splines. We also fit equivalent continua to 77 artificial spectra that we made to match the real spectra in all obvious ways: redshift, resolution, S/N, emission lines and absorption lines. The typical relative error in our continuum fits to the artificial spectra is 3.5%. Averaged over all 77 QSOs the mean level is within 1–2% of the correct value, except at S/N < 6 where we systematically placed the continuum too high. We then adjusted the continua on the real spectra to remove this bias as a function of S/N and a second smaller bias. Absorption from all lines in the Ly α forest at $z = 1.9$ removes $DA(z=1.9) = 15.1 \pm 0.7\%$ of the flux at rest frame wavelengths $1070 < \lambda_r < 1170 \text{ \AA}$. This is the first measurement using many QSOs at this z , and the first calibrated measurement at any redshift. Using similar methods on $1225 < \lambda_r < 1500 \text{ \AA}$ we find metal lines absorb an average 1.6% the flux, increasing slightly as the rest frame wavelength λ_r decreases because

¹Based on data obtained with the Kast spectrograph on the Lick Observatory 3-m Shane telescope.

²E-mail: tytler at ucsd.edu

more types of spectral lines contribute and there is more C IV at lower redshifts. We estimate that the metal lines absorb $2.3 \pm 0.5\%$ of the flux in the Ly α forest at $z=1.9$. The absorption from Ly α alone then has $DA = 12.8 \pm 0.9\%$. The Ly α lines of Lyman limit systems with column densities $\log N_{\text{HI}} > 17.2 \text{ cm}^{-2}$ are responsible for a $DA = 1.0 \pm 0.4\%$ at $z = 1.9$. These lines arise in higher density regions than the bulk of the IGM Ly α absorption, and hence they are harder to simulate in the huge boxes required to represent the large scale variations in the IGM. If we subtract these lines, for comparison with simulations of the lower density bulk of the IGM, we are left with $DA = 11.8 \pm 1.0\%$. The mean DA in segments of individual spectra with $\Delta z = 0.1$, or 153 Mpc comoving at $z = 1.9$, has a large dispersion, $\sigma = 6.1 \pm 0.3\%$ including Lyman limit systems (LLS) and metal lines, and $\sigma(\Delta z = 0.1) = 3.9^{+0.5}_{-0.7}\%$ for the Ly α from the lower density IGM alone, excluding LLS and metal lines. This is consistent with the usual description of large scale structure and accounts for the large variations from QSO to QSO. Although the absorption at $z = 1.9$ is mostly from the lower density IGM, the Ly α of LLS and the metal lines are both major contributors to the variation in the mean flux on 153 Mpc scales at $z = 1.9$, and they make the flux field significantly different from a random Gaussian field with an enhanced probability of a large amount of absorption. We find that a hydrodynamic simulation on a 1024^3 grid in a 75.7 Mpc box reproduces the observed DA from the low density IGM alone when we use popular parameters values $H_0 = 71 \text{ km s}^{-1}\text{Mpc}^{-1}$, $\Omega_b = 0.044$, $\Omega_m = 0.27$, $\Omega_\Lambda = 0.73$, $\sigma_8 = 0.9$ and a UV background (UVB) that has an ionization rate per H I atom of $\Gamma_{912} = (1.44 \pm 0.11) \times 10^{-12} \text{ s}^{-1}$. This is 1.08 ± 0.08 times the prediction by Madau, Haardt & Rees (1999) with 61% from QSOs and 39% from stars.

1. Introduction

Our physical understanding of the IGM comes from the detailed comparison of numerical simulations of the growth of structure in the universe with observations of the Ly α absorption from the H I in the IGM. The amount of Ly α absorption depends on a combination of at least four factors: the mean density of H in the IGM, the power spectrum of the matter distribution that determines the amount of clumping of the H on various scales, the temperature of the gas, and especially the mean intensity of the UVB radiation that photoionizes the gas. Together these parameters, and their variation, give the density of H I down the line of sight to a QSO, something we observe with Ly α absorption.

The mean amount of absorption is a sensitive measure of the physical properties of the IGM. If we make some assumptions about the growth of structure and the temperature of the IGM, then the optical depth of the Ly α forest scales like (Rauch et al. 1997, Eqn. 17)

$$\tau_{\text{Ly}\alpha} \propto (1+z)^6 H(z)^{-1} (\Omega_b h^2)^2 T^{-0.7} (\rho / \langle \rho \rangle)^\alpha \Gamma_{912}^{-1}, \quad (1)$$

where ρ is the proper baryon density, Γ_{912} is the photoionization rate per H I atom, and T is the gas temperature. The exponent $\alpha = 2$ for isothermal gas, and it is 1.6 – 1.8 for the low density IGM, because denser gas is hotter (Hui & Gnedin 1997; Croft et al. 1997, 2002a). To first order, the amount of absorption at a given wavelength in a spectrum reflects the density of H I in part of the IGM, which comes from the density of gas and dark matter.

Many authors have used this relationship, together with an estimate of Γ_{912} , to estimate the cosmological baryon density from the mean amount of absorption in the Ly α forest. The $\Omega_b h^2$ estimates have all been too large (Haehnelt et al. 2001, Fig. 4). Rauch et al. (1997) estimated $\Gamma_{912} > 7 \times 10^{-13} \text{ s}^{-1}$ due to the contribution to the UVB from known QSOs, which is consistent with the $\Gamma_{912} = 8.15 \times 10^{-13} \text{ s}^{-1}$ due to QSOs from Haardt & Madau (1996). This corresponds to $\Omega_b h^2 > 0.021$ in a Λ CDM model. Steidel et al. (2001) found that a large fraction of ionizing photons escape from Lyman break galaxies, giving $\Gamma_{912} > 1.5 \times 10^{-12} \text{ s}^{-1}$. Haehnelt et al. (2001) used this to conclude $\Omega_b h^2 > 0.06$ in their Λ CDM models, while Hui et al. (2002) assumed different mean temperature for the IGM and found $\Omega_b h^2 = 0.045 \pm 0.008$. These values are higher than the more robust measurements of $\Omega_b h^2 = 0.021 \pm 0.002$ from our measurements of D/H using Standard Big Bang Nucleosynthesis (Kirkman et al. 2003), and $\Omega_b h^2 = 0.0224 \pm 0.0009$ from the anisotropy of the CMB (Spergel et al. 2003). In this paper we present a more accurate measurement of the mean amount of absorption in the Ly α forest, DA, and for the first time we find that this is consistent with $\Omega_b = 0.044$ in a popular cosmological model.

An accurate measurement of DA is also a critical input to the measurement of the power spectrum of matter using the Ly α forest (Croft et al. 2002b). This is because a smaller DA requires a larger amplitude for the matter power spectrum, if all other factors are unchanged. The larger the matter power amplitude, the less gas is left widely distributed in the IGM where it causes the most absorption. For a given simulation, DA determines the relationship between the mass field and the Ly α forest optical depth – which we use to infer the Ly α forest mass power spectrum from the Ly α forest flux power spectrum. Hence, DA can be used to fix the constant of proportionality in Equation 1 above. DA also has an effect on the shape of the power spectrum deduced from the Ly α forest (Zaldarriaga et al. 2003, Seljak et al. 2003, Figure 1b).

Whether the power spectrum measured by the Ly α forest might have lower amplitude than that expected from measurements on larger scales from galaxies and the CMB (Spergel

et al. 2003) depends upon the accuracy of the Ly α forest DA measurements. Croft et al. (2002b) stressed that the uncertainty in DA is the main source of error in estimates of the matter power spectrum from the Ly α forest. Their Figure 17 shows how the amplitude of the matter power spectrum changes with the mean opacity, for a fixed flux power. They chose $\tau_{\text{eff}}(z = 2.72) = 0.349$ from Press et al. (1993). If instead we now choose $\tau_{\text{eff}}(z = 2.72) = 0.280$, from the right hand of Figure 1 of Schaye et al. (2003), which we expect is more accurate, the Croft et al. (2002b) results show that the matter power spectrum rises by a factor of 2.1, assuming no change to the temperature-density relation in the IGM. Seljak et al. (2003) also discussed this situation in detail. They reviewed DA estimates and chose $\tau_{\text{eff}}(z = 2.72) = 0.298$, from McDonald et al. (2000). They too find that this change increases the matter power by a factor of two compared to the value in Croft et al. (2002b), when combined with an increase in the slope of the matter power spectrum.

Croft et al. (2002b, Eqn. 12) find that the 3D matter power spectrum amplitude $\propto \tau_{\text{eff}}^{-3.4}$, for a given observed flux power. This implies that to measure the power spectrum amplitude to 10% at this z , we would need a relative error on τ_{eff} of 3%, which is a relative error on DA of 2.4%, assuming that all other factors were well known, which is not the case. We find a similar scaling relation from Seljak et al. (2003).

However Gnedin & Hamilton (2002, Eqn. 8) find a much weaker correlation between the matter power and DA. Although the origin of this disagreement is unknown, Seljak et al. (2003) suggest that Gnedin & Hamilton (2002) did not sample a wide enough range of parameters. Larger amplitude power comes with higher velocities which decreases the flux power on small scales. As the matter power increases, the flux power can both rise on large scales and fall on small scales.

These results show that high accuracy DA measurements are of great interest because of their cosmological significance. In general, accurate measurements of DA can become a cornerstone in a concordance model of the IGM, tying together the intensity of the UVB, the thermal history of the IGM and the cosmological matter power spectrum.

1.1. Definition of DA

Following Oke & Korycansky (1982) we define $DA = 1 - \langle F \rangle$ where $\langle F \rangle = (\text{observed flux})/C$, $C = (\text{estimated unabsorbed continuum flux})$ which includes both the underlying power law and the flux from emission lines. It is common to see DA expressed as $\langle F \rangle$, or as the mean effective optical depth, $\tau_{\text{eff}} = -\ln \langle F \rangle$.

We will measure DA in individual pixels, and we will use suffixes on the DA to la-

bel averages over various wavelengths between the Ly α and Ly β emission lines, sometimes averaged over many QSOs. We restrict our measurement of DA to rest frame wavelengths

$$\text{DA wavelength range} = 1070 \text{ to } 1170 \text{ \AA}. \quad (2)$$

The DA is dominated by Ly α lines from the IGM, but it includes all absorption, including metal lines and the Ly α lines from LLS that by definition include all damped Ly α lines (DLAs).

After we measure DA, we will give estimates for the amount of absorption due to the Ly α lines of high column density absorption systems and metal lines, both of which are harder to simulate.

1.2. Prior Measurements of DA

More than a dozen papers contain measurements of DA: see references in Rauch (1998) and Bernardi et al. (2003) and the discussion of errors in Croft et al. (2002b) and Seljak et al. (2003).

DA is hard to measure because we need many QSO spectra, the unabsorbed continuum level is hard to estimate, and when we want just the H I portion of the DA, the metal lines in the Ly α forest are difficult to find and measure.

To measure the mean DA with a relative error of 1%, i.e. $\text{DA} = 0.300 \pm 0.003$, in a specific redshift range, we must observe about 10,000 Ly α lines with N_{HI} values similar to those that makes most of the optical depth (Kirkman & Tytler 1997, Fig. 8). We need of order 500 QSOs at $z = 3$. Most samples have used under ten QSOs.

The unabsorbed continuum is relatively easy to find in high resolution spectra with high S/N, but we have few of these spectra. Instead, the continuum in the Ly α forest has often been set to a power law extrapolated from wavelengths $> 1250 \text{ \AA}$, and this can be biased (Kim et al. 2001; Meiksin et al. 2001; Seljak et al. 2003).

Most papers have not attempted to find and remove metal lines. Instead they include such lines in their DA values.

These difficulties have lead to large differences in reported DA values. Jenkins & Ostriker (1991) noted that the distribution of flux in the Ly α forest region implies that there is about 30% more absorption than is expected from lines identified in spectra, which is a huge uncertainty. Meiksin (1997, private communication) long ago drew our attention to these disagreements. For example, at $z \simeq 3$ we have $\tau_{\text{eff}} = 0.28, 0.38$ and 0.45 from Hu et al. (1995);

Rauch et al. (1997) and Press et al. (1993) respectively, while at $z = 2.72$ we have $\tau_{\text{eff}} = 0.28$ from Schaye et al. (2003) and 0.35 from both Press et al. (1993) and Bernardi et al. (2003).

The uncertainty over DA has hindered attempts to measure parameters such as Ω_b from the Ly α forest. Zhang et al. (1998) obtained DA from a conventional power law fit to the N_{HI} distribution fit from Hu et al. (1995), who in turn had used Keck spectra of 4 QSOs all at $z = 3.1 - 3.4$. We know that the integral over this power law could contain large errors. Weinberg et al. (1997) used Press, Rybicki & Schneider (1993) very low resolution (25Å) spectra of 29 QSOs at $z = 2.5 - 4.3$. We will discuss the most detailed study, by Rauch et al. (1997) later.

Two recent measurements of DA are of special interest. Bernardi et al (2003) used 1061 SDSS spectra to measure DA at $2.6 < z_{\text{abs}} < 4.0$, again outside our range. They introduce new methods and obtain by far the best random error although there seem to be systematic problems with their results. Schaye et al. (2003) used 21 UVES and HIRES spectra, with $S/N > 40$ and they removed metal lines. They found τ_{eff} values that are systematically lower than Bernardi et al. (2003) by 0.1 dex.

1.3. What we will do

Using artificial spectra with similar characteristics to the Kast spectra set (e.g. S/N, resolution, redshift, and continuum shape), we will characterize and statistically account for errors such as continuum placement. We will aim for an absolute error in the mean DA value of $< 1\%$, dominated by the random noise coming from the sample size.

The paper is organized as follows: in §2 to §5 we describe our data set and calibration methods. In §2 we describe the Kast spectra; in §3 we describe the artificial spectra that we created to calibrate the continuum fit; in §4 we describe the continuum fits; and in §5 we measure and correct the errors we made in the continuum fits.

In §6 to §15 we describe the results of our DA measurement. In §6 we give our measurement of DA. In §9 we describe the dispersion we see in DA, and in §11 we summarize the error on DA. In §15 we summarize and discuss our results.

To convert from redshift to distance, we use a Hubble constant $H_0 = 71 \text{ km s}^{-1} \text{ Mpc}^{-1}$, a vacuum energy of $\Omega_\Lambda = 0.73$, and a matter density of $\Omega_m = 0.27$ and we evaluate at $z = 1.9$.

2. Kast QSO Spectra

We obtained spectra of the Ly α forest of bright QSOs at $1.85 < z_{\text{em}} < 2.5$. We maintained a list of all such QSOs listed in NED, and updated it before each observing run. We found about 6000 QSOs of all magnitudes. We rejected those noted as BAL in NED, and we then observed the brightest remaining at declination North of -30 degrees. Most were 17th magnitude. We observed nearly all that were brighter than 17.5 and some that were 18th magnitude. We rejected BAL QSOs because they tend to show much more absorption than other QSOs. In the Ly α forest region this absorption is from N V, and other ions. BAL QSOs would also bias our estimates of the mean amount of metal line absorption because they can have huge amounts of C IV and Si IV absorption.

2.1. Observations

We obtained spectra from 2001 January 26 to 2003 July 28 with the Kast double spectrograph on the Shane 3m telescope at Lick observatory. Here we discuss spectra obtained with the blue camera, using the grism with 830 groves per mm, blazed at 3460 \AA , and covering approximately $3150 - 4300 \text{ \AA}$. We also took simultaneous spectra with the red camera with the 1200 grove/mm grating blazed at 5000 \AA , giving 1.17 \AA /pixel and covering 4400 \AA to the red of C IV emission. We will not discuss those red spectra here.

We used the slit that is 2 arcsec wide when the seeing was good, but a 3 arcsec or wider slit was sometimes necessary. The slit was aligned with the vertical direction on the sky in the middle of each exposure.

We know from prior work with this instrument (Suzuki et al. 2003) that the typical dispersion is $1.13 \text{ \AA per /pixel}$ (107 km s^{-1}), and the FWHM resolution is 250 km s^{-1} (2.5 pixels), with a range of $200 - 300 \text{ km s}^{-1}$, depending on the temperature and the focus that we chose for that observing run. The spectral resolution varies with wavelength, and from run to run, even when the slit is unchanged.

2.2. Reductions

We extracted and reduced the spectra with the standard IRAF long slit reduction packages. We performed the wavelength and flux calibrations in the standard manner, again using IRAF. We gave a detailed discussion of similar reductions of spectra from the same instrumental setup in Suzuki et al. (2003). Wavelength errors are typically under 1 \AA . The

standard extinction correction was applied, but we have not performed a separate correction for the fluctuations in the ozone absorption. We calibrated the flux using Kast spectra (taken on the same night as the QSO spectrum) of one or more of the following flux standard stars: BD+28 4211, BD+33 2642, Feige34, Feige67 and G191b2b. We took the fluxes for these stars from HST spectra that we have shown are ideal for the wavelengths of interest (Suzuki et al. 2003). In a few cases we found that calibrations using different stars differed.

We changed the flux in the occasional pixel that was clearly erroneous because of poor cosmic ray or sky subtraction. We set such pixels to the expected level, to reduce the effect on the continuum fitting and the DA estimate. Hence the spectra are cosmetically unusually clean.

2.3. QSO Sample used

We attempted to set the integration times to reach $S/N = 10$ per pixel at 3200 \AA , although weather sometimes prevented us from achieving this. The S/N in the continuum of the spectra from $\text{Ly}\beta$ to $\text{Ly}\alpha$ vary from a few to over 50, with typical values of $6 - 20$. Some of this variation is from QSO to QSO, at a given wavelength, and some is variation with wavelength within each spectrum. For all spectra, the S/N increases systematically with wavelength, and hence with z_{abs} . This has important consequences that we discuss below.

We rejected about 10 QSOs because the SNR was < 2 . We rejected Q2310+0018 (RA 23h10m50.80s +00d18m26.4s B1950, $z_{\text{em}} = 2.200$ mag. 17.00) because we discovered that it shows BAL absorption. The spectra that we obtained for 6 objects were not QSOs. Two were probably our error in pointing the telescope. It is possible that several of the other four are not QSOs: Q1456+5404, 14h56m47.71 +54d04m25.6 $z_{\text{em}} = 2.300$ 16.50mag; Q1742+3749, 17h42m 5.55 +37d49m08.3 $z_{\text{em}} = 1.958$ 16.40mag; Q1755+5749, 17h55m15.97 +57d49m06.9 $z_{\text{em}} = 2.110$ 18.00mag; and Q2113+3004, 21h13m59.42 +30d04m02.4 $z_{\text{em}} = 2.080$ 17.30mag.

After these various rejections we are left with $\text{Ly}\alpha$ forest spectra of 77 QSOs, which we use in this paper. We measured the z_{em} for each QSO from the emission lines in its blue spectrum, typically $\text{Ly}\alpha$, Si IV and C IV.

In Figure 1 we show a histogram of the z_{em} values, and the number QSOs contributing $\text{Ly}\alpha$ forest information at various z_{abs} values. The mean $z_{\text{em}} = 2.17$ while the mean $z_{\text{abs}} = 1.924$. Had we weighted by S/N , the mean z_{abs} would have been > 2 . We use spectra with observed wavelengths $3173 - 4083 \text{ \AA}$ with a range of $\pm 5 \text{ \AA}$ from the precise CCD placement. This corresponds to $z_{\text{abs}} = 1.6105 - 2.3587$ for $\text{Ly}\alpha$. Eight of the QSOs with $z_{\text{em}} < 1.965$ do not cover the whole $1070 - 1170 \text{ \AA}$ range, since their 1070 is $< 3173 \text{ \AA}$.

When we use the entire sample to measure DA, which we will call DA4, we sample a total redshift path of 19.750 (30.8 comoving Gpc) in 23,000 pixels of 1.13 Å in the observed frame. At a redshift of 1.9, one pixel corresponds to 1.56 comoving Mpc, for a model with $H_0 = 71 \text{ km s}^{-1}/\text{Mpc}$, $\Omega_\Lambda = 0.73$, and $\Omega_m = 0.27$.

3. Artificial QSO Spectra

We have made a set of 77 artificial spectra, each one matched to one of the Kast spectra. Each artificial spectrum has the same z_{em} and S/N distribution as one of the Kast spectra. All the artificial spectra have shapes, including emission lines, from real HST spectra of lower redshift QSOs, they all have random Ly α absorption lines from simulations of the IGM, and they have the same spectral resolution as the Kast spectra.

The starting point for the artificial spectra were the smoothed absorption free fits to the continuum and emission lines of the 50 QSOs discussed and listed in Table 1 of Suzuki et al. (2004a). They have $0.14 < z_{\text{em}} < 1.04$ and an average S/N = 19.5 per 0.5 Å in the rest frame from 1050 – 1170 Å. The HST continua on these spectra had previously been adjusted to match our understanding of QSO continua. We believe that the continua levels are better known than those for the Kast spectra, because the S/N is relatively high and there are far fewer absorption lines at these low redshifts. In a quick look, the shapes of these HST spectra are not obviously different from those of the QSOs that we observed with the Kast spectrograph.

We randomly associated each of the HST spectra with one of the Kast spectra, and we use 27 of the HST spectra twice. These associations match each of the z_{em} values to one and only one of the artificial spectra. We trimmed wavelength range of each artificial spectrum to match the range of its paired Kast spectrum.

Next, we added Ly α absorption from heuristic simulations of the Ly α forest. The model used for the forest is a simplified version of the Bi et al. (1992) log-normal model, which incorporates non-linear effects into the linear theory of structure formation. In the log-normal model, the transmission fraction field is simply defined to be

$$F(\lambda) = \exp \left(-\tau_0 \exp \left[\delta(\lambda) - \sigma^2/2 \right]^2 \right) , \quad (3)$$

where $\delta(\lambda)$ is a Gaussian random field. The power spectrum of δ , $P_\delta(k)$, was constructed to make the simulated power spectrum of F , $P_F(k)$, roughly match the observed $P_F(k)$ (e.g., from McDonald et al. (2000)). We made $\tau_0(z)$ and the amplitude of $P_\delta(k, z)$ slowly varying functions of redshift to match observations. The change in the total absorption due to Ly α

in these simulated spectra should follow $A(1+z)^\gamma$, where $A = 0.0166$ and $\gamma = 2.07$. The simulations were made with full numerical resolution, and then smoothed to a FWHM of 250 km s^{-1} .

We added the absorption starting at 1215.67 \AA (rest frame, as are the rest of the wavelengths in this section). This is typically near the peak of the $\text{Ly}\alpha$ emission line using the z_{em} value that we had measured. The absorption was added by multiplying the smoothly changing fit to the HST spectrum by flux values from $0 - 1$. We continued the absorption down to the UV end of the spectrum. The spectra contain only $\text{Ly}\alpha$ absorption, even when we are at wavelengths where $\text{Ly}\beta$ would also appear in Kast spectra. We did not make any adjustments for the proximity effect, and hence the absorption from the $\text{Ly}\alpha$ forest in the artificial spectra begins at exactly 1215.67 \AA .

These simulations produce $\text{Ly}\alpha$ forest absorption that is similar to Kast spectra, but they were not adjusted to be as close as possible. Compared to Kast spectra, the simulations have too few $\text{Ly}\alpha$ with large equivalent widths coming from the LLS, and they have no DLAs. Otherwise, by visual inspection alone, we can not tell the artificial spectra from the real $\text{Ly}\alpha$ forest. The lack of a proximity effect region is not a distinction, since this can not be seen in a single spectrum.

We added a Gaussian random deviate to each pixel in each artificial spectrum to make its S/N similar to that of its partner. This procedure is complicated because we wish to simulate the S/N that we would have obtained with Kast, had we observed the QSO with the z_{em} of its partner and the spectral slope and emission lines of the HST spectrum. Hence we can not simply copy the S/N from the Kast spectrum partners, because the emission lines differ.

The S/N that we gave to an artificial spectra had the same values as the S/N in its partner spectrum at two reference wavelengths, 1100 and 1255 \AA , and it responds to emission lines according to the $\sqrt{\text{flux}}$ in the artificial spectrum.

In detail we multiplied the flux in each artificial spectrum by the response function of the Kast, to simulate the distribution of photons that we would have recorded, had we observed the HST flux distribution. The square root of this gives the relative S/N as a function of wavelength. We then measured the S/N in both the artificial and Kast spectra averaging over 0.02 in z (24.3 \AA rest) around each reference wavelength. We took the ratios of these S/N values, Kast upon artificial, to derive correction factors. We fit a straight line between the two correction factors and then multiplied the S/N on the artificial spectrum by this line. The artificial and Kast spectrum then have the same S/N at the reference wavelengths, and generally similar distributions of S/N with wavelength. We checked that the distribution of

S/N in the DA region in the 77 artificial spectra was very similar to that in the 77 Kast spectra.

In Figure 2 we show two artificial spectra. The only easy way to see that these are artificial is that there is zero absorption to the red of Ly α .

4. Continuum fitting

The methods that have been used to estimate the unabsorbed continuum in the Ly α forest fall into two general classes:

- Extrapolations from wavelengths $> 1250 \text{ \AA}$ (rest frame, as are the other wavelengths in this section) that do not use the flux information from the Ly α forest. The extrapolations use power laws (Oke & Korycansky 1982; Steidel & Sargent 1987; Bernardi et al. 2003), similar smooth functions (Press et al. 1993), or principal components that also predict the shapes of emission lines in the Ly α forest (Suzuki et al. 2004a).
- Fits to the local continuum in the Ly α forest that emphasize the wavelengths with the most flux (Rauch et al. 1997; Fang et al. 1998; McDonald et al. 2000; Kim et al. 2002; Schaye et al. 2003).

The values that we quoted in §1 illustrate that the extrapolations give systematically much more DA than do fits to the local continuum, a point noted by others (Kim et al. 2001; Meiksin et al. 2001; Seljak et al. 2003). Like other authors, we suspect that the extrapolated continua are less reliable, and too high in the Ly α forest.

Seljak et al. (2003) suggest that the extrapolated continuum is too high because QSO spectra are not well fit by a power law with a single slope. It is well established that best fit power law declines faster with decreasing wavelength at < 1200 than at $> 1300 \text{ \AA}$ (Telfer et al. 2002, Figure 4). Seljak et al. (2003) calculate that the DA from power law extrapolations should be decreased by least 0.05 to correct this bias. The precise correction will depend on how and where the power law fit was made to the spectra, since there are many strong blended emission lines at $> 1250 \text{ \AA}$.

A second reason why the extrapolations might be biased is that shape of the typical QSO spectrum in the Ly α forest is much more complex than a pair of power laws. Figure 5 of Press et al. (1993), Figure 6 of Vanden Berk et al. (2001), Figures 4 & 9 of Telfer et al. (2002), Figure 3 of Bernardi et al. (2003) and Figures 2 & 3 of Suzuki et al. (2004a) all clearly show that the region from Ly β -O VI to Ly α is dominated by the wings of those two

emission lines, and by lines near 1073 Å (possibly blend of N II, He II and Fe II, according to Telfer et al. 2002, or Ar I according to Zheng et al. 1997) and 1123 Å (Fe III). In some spectra 1073 and 1123 are weak, but in the mean spectrum they are strong enough that all wavelengths are influenced by one or more of these four lines, separated by three flux minima, near 1050, 1100 and 1150 Å. The flux minimum near 1050 Å between Ly β and 1073 Å is especially hard to recognize in spectra with a lot of absorption or low S/N, and although we were looking for it, in some cases we missed it, as in the left panel of Figure 2.

There are also weaker emission lines near 1176 Å (C III*, Vanden Berk et al. 2001; Telfer et al. 2002; Suzuki et al. 2004a), and possibly 1195 (Si II, Telfer et al. 2002) and 1206 Å (Si III, our HIRES spectrum) all in the wings of the Ly α line, and outside our DA region.

The sign of the bias in the continuum that comes from ignoring these lines will depend on the details of the continuum extrapolation or fit, and in the case of a fit, on whether the person making the local continuum fit was aware of these lines, attempted to fit them, and had spectra of wavelengths > 1216 Å where other emission lines suggest the likely strengths of the Ly α forest lines.

Bernardi et al. (2003) were the first to call attention to the emission lines near 1073 and 1123 Å, and they fit QSO continua with power law plus three Gaussian functions, one each for these lines and Ly α .

In Suzuki et al. (2004a) we used principal component analysis to predict the shape of the Ly α forest continuum and emission lines in individual spectra, using the shape of the spectrum at wavelengths 1216 – 1600 Å. The results were sometimes excellent, but other times poor, in part because of the sensitivity to the flux calibration. The predicted flux in the Ly α forest of a QSO had an average absolute error of 9%, with a range from 3 – 39%, which is too large an error for a DA measurement, especially since we do not know whether the mean is systematically too high or too low.

Amongst the methods that use the local flux in the Ly α forest we note Fang et al. (1998) who used the mode of the distribution of flux to estimate the continuum level on our HIRES spectrum of one bright QSO. This works best when the S/N is very high and the spectral resolution is high enough to show regions with minimal absorption, neither of which is the case for our Kast spectra.

4.1. The Local Continuum Fits that we made

The method that we use to fit continua is that normally used on high resolution spectra with high S/N: fitting a different smooth curve to each Ly α forest spectrum. This method is routinely used for measurements of absorption lines, and for DA when the spectra have high resolution, high S/N, and the z_{abs} is low enough that there are some regions that appear to be absorption free.

Rauch et al. (1997) fit local continua to Keck HIRES spectra of 7 QSOs at $z_{\text{em}} = 2.5 - 4.6$ that differed widely in S/N. They used spline fit continua with rejection of 3σ depressions. They corrected their continua upwards because some regions lack pixels without absorption. The corrections came from the highest flux in each simulated spectrum, from a box $10h^{-1}$ comoving Mpc long for a Λ CDM model. At $z = 2$ this correction was small, from DA = 0.148 to 0.154. We shall also use artificial spectra make corrections to the whole of each QSO spectrum.

McDonald et al. (2000) fit local continua to the same spectra used by Rauch et al. (1997) plus one more. They used IRAF to fit Spline3 or Chebyshev polynomials to the continua, which were cut into 2 – 4 pieces prior to the fits. They fit to the flux in portions of the spectra that seemed free of absorption, with various orders of polynomial. The fits were complicated because the flux calibration was not good. Schaye et al. (2003) also fit local continua to 22 UVES and HIRES spectra.

We know from our work on D/H measurement that we can fit the Ly α forest continuum in high S/N HIRES spectra with an error of around 2% (Kirkman et al. 2003). We fit a smooth curve by eye, using a b-spline as a convenient way to store the result. This motivated us to try to use and calibrate the same method on the Kast spectra. We find that the method works because the lower spectral resolution is compensated by the much lower density of Ly α lines at $z \simeq 1.9$, and because we have a large wavelength range, extending to near C IV, in each spectrum.

We used a b-spline fit to each spectrum that started with one control point every 50 Å. We added points, especially in the emission lines, and we manually adjusted all points over the entire spectrum to obtain our best guess at the unabsorbed continuum. The continuum is strongly influenced by the observed flux levels throughout a spectrum, and by our perception of the strengths and shapes of all the emission lines throughout the spectrum. We did not explicitly assume that any particular part of a spectrum was absorption free.

We paid close attention to the emission lines, especially those at 1073 and 1123 Å (Suzuki et al. 2004a). We sorted the spectra according to the strength of these lines, and we attempted to produce a consistent set of lines across the whole of each spectrum, out

to C IV. We found that strong lines such as Si II 1263, O I/Si II 1306 and C II 1335 often indicated strong lines near 1073 and 1123.

Two of us reviewed the entire set of fits to the Kast and artificial spectra all in one sitting, to try to make a consistent set of fits for the entire sample. We repeated this exercise after we had made the corrections following the first review.

4.2. Errors in our Continuum Fits

We now examine the errors in the continua that we fit to the artificial spectra. In each case we know the true continuum level. We will make the important assumption that the continua on the Kast spectra have similar errors.

To measure the error in our continuum fits, we define

$$F1/TC = (\text{fitted continuum})/(\text{true continuum}). \quad (4)$$

We measured F1/TC for each pixel in each artificial spectrum. The mean of the absolute fractional error in our continuum fits in the DA region is 3.5%. At a random wavelength in a random QSO, 16% of the pixels have $F1/TC > 1.051$, and 16% have $F1/TC < 0.970$. The standard deviation of F1/TC is about 5.4% in the DA wavelength range. At 1216 – 1500 Å the F1/TC standard deviation is 1.7%.

In Figure 2 we show our F1 continuum fits to two artificial spectra. For each we show both the true and the fitted F1 continuum and the ratio F1/TC. These spectra illustrate several errors typical of the continuum fits. We often underestimate the amount of absorption near the peak of the Ly α line (right spectrum). We were aware of this possibility but we still failed to anticipate the full effect. We also failed to give the emission lines enough structure. For the left hand spectrum we failed to drop down between the Ly β – O VI blend and the line at 1073 Å that can be almost as high as Ly β .

Although the S/N is higher in emission lines, the uncertainty in their shape more than compensates. On average, the dispersion in F1/TC is slightly larger in the emission lines. In some QSOs the emission lines have typical F1/TC (left spectrum in Fig. 2), but in others the Ly α line has the largest continuum error of anywhere in the spectrum (right spectrum). Errors are also larger at the UV end of spectra where the S/N is lowest.

We classify our fits around the Ly α emission line peak as follows. For 34 QSOs the fits are good to excellent, and no worse than elsewhere in the Ly α forest. For 31 we fit too low, usually over a single region 3-10 Å (rest) wide (like the right spectrum in Fig. 2), but sometimes over wider region. For 3 QSOs we fit too high, and for 9 we fit one region too

high and another too low. We considered and rejected using this knowledge to adjust our continua on both the artificial and Kast spectra, because it would not change our results.

The errors in the continuum fits were correlated over a variety of lengths, determined by the number of b-spline points that we chose to use. We typically could justify using more points where the S/N was high in the Ly α forest, in the red, and where there are many pronounced emission lines. Although there was no particular scale of correlation, we often saw strong correlations over 10–40 Å in the rest frame in the Ly α forest region for most spectra and over a few Å in the Ly α line.

The continua on some of the artificial spectra are poor, with errors of 10 – 20%, all across the Ly α forest. Of the four with the largest errors, two have low S/N, but two others have intermediate S/N \simeq 5.

5. Correcting the Continuum Levels using the Artificial Spectra

We measured DA in the DA wavelength range: 1070-1170 Å. We examined plots of our Kast spectra, stacked in rest wavelength, to help us make these choices. We chose these wavelengths to avoid the proximity effect, the wings of Ly α where the continuum is changing rapidly, the Ly β – O VI blend (1025.72, 1031.9, 1037.6 Å) and the local flux minimum near 1050 Å that is hard to recognize. Associated absorption that was falling towards the QSO at -3000 km s $^{-1}$ (near the maximum velocity ever seen) would have its O VI 1037 at 1048.09 Å. In some spectra the continuum fits get noticeably worse at < 1070 Å, and we will see that the standard deviation increases at < 1070 Å. For a Ly α line, $\lambda_r = 1170$ Å is 11300 km s $^{-1}$ or 170 comoving Mpc from a QSOs at the mean z_{em} , sufficiently far that we do not expect a significant influence from the observed QSO. Later in this section we will see that we systematically fit the continuum too low in the range 1170 – 1216 Å.

The mean of the DA values in all pixels in the artificial spectra, averaged over the DA region wavelengths and all artificial spectra, and using the true continua, is 0.1601. This value applies to a mean Ly α $z = 1.924$.

5.1. Correcting the continua of the Artificial Spectra using SNR2

We defined a new variable, SNR2, to act a measure of the effect of photon noise on the data quality. It is an indicator of the data quality on large scales, and represents the smoothed S/N that we would have measured in absence of absorption and emission lines. We ignore both absorption and emission lines because to first order we do not expect our

continuum level estimates to be better or worse near a narrow absorption line and we found that the continuum fits are slightly worse in the emission lines.

We defined SNR2 as a smoothly varying function of wavelength, with values similar to the S/N at those wavelengths. It is not smoothed S/N, since this is depressed by absorption lines. Rather it is the flux and S/N in the relatively unabsorbed regions of the spectrum that most influence the continuum fitting accuracy. SNR2 is a linear fit to the S/N values that we measured at the two reference wavelengths.

In Figure 3 we show F1/TC as a function of SNR2. We show the mean F1/TC for all pixels (often over 1000) in a given SNR2 range, and we use all pixels from 1050 – 1070 Å, which extends to 20 Å lower wavelengths than the DA region. The means show correlation between adjacent bins, since the F1/TC in the spectra are also correlated over tens of Å, and hence over a range in SNR2, which varies smoothly with wavelength. The plot shows that the F1 continua are systematically too high at $\text{SNR2} < 6$, and usually too low at $\text{SNR2} > 12$. This type of error is not unexpected.

We made new continua, labelled F2, by dividing the F1 continua on both the Kast and artificial spectra by the factors shown in Figure 3.

The correction worked as expected on the artificial spectra. The DA we measured using the initial continua F1 was 0.1687, significantly too large. The DA measured using the F2 continua was 0.1585, which is 0.990 of the value for the input artificial spectra: 0.1601. The DA4(F1) was too large by 5.2%. We checked that when we applied the correction to 1050 – 1170 Å the total DA was 0.1583, which is 0.1% less than the DA = 0.1585 for this wavelength range in the input artificial spectra.

The effect is similar for the Kast spectra: We had DA = 0.1637 using the F1 continua, and we find DA = 0.1533 using the F2 continua. DA(F1) was too large by 6.8%, similar to the excess for the artificial spectra, but not identical because the distribution of flux as a function of SNR2 is different.

5.2. Correcting the continua of the Artificial Spectra using SDA

We define a second variable which also indicates regions of the spectra where we might have made systematic errors in the continuum fits. SDA is smoothed DA, obtained by smoothing the flux with an exponential filter with FWHM 25 Å rest. This length is similar to the scales on which we see strong correlations in the continuum errors.

In Figure 4 we show the F2/TC as a function of SDA. We see a systematic trend that

indicates that F2 is too high by about 1% on average in regions of the artificial spectra that have $0.3 < \text{SDA} < 0.6$. We used the smooth curve to approximate the corrections that we made to F2 to remove this trend. We show how we extrapolated the curve to higher SDA values that occur in some parts of the Kast spectra, but not in the artificial spectra, because the artificial spectra differ from the Kast spectra.

We label F3 the continua that we corrected for the SDA correlation (F2 to F3) after we had corrected them for the SNR2 correlation (F1 to F2). For the artificial spectra, the mean DA following the correction to F2 was 0.1585 and after the correction using SDA the F3 continua gave DA 0.1602. The change is 1.1%, and leaves the DA nearly identical to the known value, 0.1601, as required by the definition of the corrections.

For the Kast spectra, the change is a 1.2% increase, from $\text{DA}(\text{F2}) = 0.1533$ to $\text{DA}(\text{F3}) = 0.1552$. This is slightly different from the change to the artificial spectra because the distribution of the flux as a function of SDA can differ from that for the artificial spectra.

In Figure 5 we see that F3/TC is a well behaved function of rest wavelength. The thick bars show the mean values, from all QSOs (usually 77) that contribute at that wavelength. The mean F3/TC across the DA region is near 1.0 by definition of the corrections. About 16% of pixels have $\text{F3/TC} < 0.96$ and 16% are > 1.03 , with little variation across the DA region. We are not surprised that the mean F3/TC values are correlated over many pixels and regions of around 60 Å because the continuum errors F1/TC were also correlated over such large scales. We also see a tendency for the F3/TC to be too low in the interval 1170 – 1216 Å. We saw that we fit the continuum too low in this region for some QSOs.

In Figure 6 we show the standard deviation of the F3/TC values, $\sigma(\text{F3/TC})$, as a function of λ_r . The value is nearly constant, around 1.3% at > 1220 Å. It peaks near the peak of Ly α , at 4.5%, declining slowly as we move down the blue wing of Ly α . It rises again below 1070 Å, reaching a level of 5 – 6%. We used this Figure to help us choose the DA region.

5.3. Effects that may remain uncorrected

Here we discuss two of several possible sources of error in our continuum estimates that the SNR2 and SDA corrections may have missed.

First, there are errors in the flux values in our QSO spectra, due to the limitations of the flux calibration procedure applied to the observed spectra. There are numerous sources for such errors, which we describe in detail in (Suzuki et al. 2003). Fortunately, many flux

calibration errors in low resolution spectra vary smoothly over large scales $> 50 \text{ \AA}$, and they will mostly have been absorbed as adjustments to the continuum fit, reducing their effect on the DA. Some of these errors might vary randomly in sign from QSO to QSO, and with wavelength, leading to a minimal net effect in our sample, but others are systematic.

An example of a systematic flux error is the strong atmospheric ozone absorption that varies in strength with a period of about 25 \AA , and increases a lot below about 3310 \AA (Schachter 1991). We did not explicitly remove the ozone absorption from either the standard stars or the QSO spectra, hence we expect to see this pattern in the Ly α forest absorption. In Figure 7 we show DA as a function of observed wavelength. Some variations can be seen at rest wavelengths $< 3250 \text{ \AA}$, which are probably due to ozone absorption. However, we note that the variations go both high and low, because we generally fit continua through ozone absorption, not above or below it, so the net effect on our estimated DA should be minimal.

Second, it is possible that the artificial spectra differ from the Kast spectra in some way that is difficult to notice, but nonetheless very important. We know that the artificial spectra lack strong Ly α lines from high density regions that have high N_{HI} . In the Kast spectra these lines alone have $DA = 1\%$. What if the Kast spectra also have some smoothly varying absorption that covers many wavelengths, but is not included in the simulations? Since we examined the whole of each spectrum, from near C IV to below Ly β , we hope that we have correctly accounted for such hypothetical absorption. However, the F3/TC will not tell us if we erred.

In summary, we are reasonably confident that we have accounted for the main systematic effects.

6. DA in Kast spectra

We applied exactly the same corrections to the Ly α forest of the Kast continua as we applied to the artificial ones to make the equivalent of F3 for the Kast spectra. We will no longer mention the uncorrected continua on the Kast spectra. Hence, the DA in a pixel, which we will label DA0, is the flux divided by the corrected continuum fit, F3. Of course we can not show you ratios like F3/TC for the Kast spectra because we do not know the true continuum levels.

In Figure 8 we show two statistics from the DA0 values. The thin vertical lines show the $\pm 1\sigma$ of the DA0 values. The center of the short solid bars show the mean DA0 from all DA0 in the 4.5 \AA rest frame wavelength regions, which we call DA1. The length of the

thick bars show the $\pm 1\sigma$ errors on those means, calculated assuming that the DA0 values were random normal deviates: $\sigma(\mu) = \sigma(DA0)/\sqrt{n}$, where the number of pixels per bin is $n \simeq 900$. We know that this underestimates the error on the mean, both because there are about 3 pixels per resolution element, and the DA0 values are far from normal deviates. We also show the DA wavelength range. We make several points from this plot that guide our decisions on how we will measure the overall mean DA4 value.

First, at 1225–1500 Å there is clearly absorption due to metal lines. The mean is around 2%, systematically increasing to smaller wavelengths. We will discuss this below.

Second, the DA1 values rises smoothly as we cross the peak of the Ly α line. The transition across the Ly α emission lines is wide, from about 1210 – 1225 Å, a range of around 3700 km s $^{-1}$. We see that the DA1 near the wavelength of the peak of Ly α (the lower end of the arrow labelled Ly α emission) is near the mean of the DA1 on either side of Ly α . This trend comes from the proximity effect, modified by the errors in the z_{em} values that we used and the large errors in continua near the peaks of the emission line. We would need to improve these two factors before we could use these data to measure the proximity effect.

Third, the DA1 is approximately constant across the DA region.

Fourth, the DA1 is higher in 1190 – 1205 Å. This might be related to the continuum fitting errors which made the F3/TC too low for 1170 – 1220 Å for the artificial spectra (Figure 5).

Fifth, the DA1 is higher at 1000 – 1045 Å. Some of this might be from continuum errors that increase as the S/N decreases. Figure 5 showed that the F3/TC values had a large σ at these wavelengths, and four of the five mean F3/TC values were slightly too high. Rather the DA1 is probably higher because of absorption by Ly β and perhaps some O VI.

Lastly, there is some extra remaining dispersion in the DA1 in the Ly α forest because we have not yet removed the tendency for DA to increase with z .

6.1. How DA Changes with z

In Figure 9 we show DA as a function of the Ly α absorption redshift. We give the values in Table 1. The thin lines are again the $\pm 1\sigma$ of all the DA0 (pixel) values in each z bin, while the thick bars show the mean DA values, $\mu(\text{DA})$ and their errors $\sigma(\mu)$, which we have underestimated. In Table 1 we also list the usual 1σ confidence interval for the DA values per pixel. We give the critical DA values, where 15.8% of the values are below the

lower value (column 4) and 15.8% are above the larger value (column 5). We see a slight increase in the DA with increasing z , as expected from well known counts of the number of lines per unit redshift, a trend first found by Peterson (1978). We fit this trend with

$$DA(z) = A((1+z)/(1+1.9))^\gamma, \quad (5)$$

with $A = 0.147$, and $\gamma = 2.57$. These values are slightly different from those for the input artificial spectra: $A = 0.150$ and $\gamma = 2.07$. We do not quote errors on these parameters because the range of z covered is very small and the slope γ is not well determined. We will concentrate instead on estimating the DA at the mean z for the sample.

7. Ly α Absorption from High Column Density Lines

Some of the absorption in the DA region is from the Ly α lines of systems with high H I column density, especially including LLS and DLAs. We now estimate how much, because these absorbers are much harder to include accurately in the numerical simulations that have the large boxes needed for the IGM. We expect that this is a temporary situation, since we would prefer to use simulations that include all the main features of the IGM and galaxies that are responsible for the absorption in QSO spectra. They should include realistic LLS and DLAs, with realistic velocity structure, temperatures and metal abundances, giving realistic metal lines.

We introduce

$$DA5(z) = N(z)W_r(1+z)/\lambda_r \quad (6)$$

as a general estimator of the amount of absorption from lines with a rest frame wavelength λ_r , a density of $N(z)$ lines per unit z and a mean rest frame equivalent width W_r (Å). The $(1+z)$ factor converts W_r to the observed frame, and for Ly α there are 1215.67 Å in the observed frame per unit z .

LLS with $\log N_{\text{HI}} > 17.2 \text{ cm}^{-2}$ have Lyman continuum optical depth > 1 (Tytler 1982) and a density $N(1.9) = 1.4 \pm 0.5$ from Figure 2 of Stengler-Larrea et al. (1995). The fractional error is huge because HST has obtained spectra of few QSOs that could show Lyman limits around 2650 Å. We measure a mean $W_r = 3.0 \pm 0.5$ Å for 66 LLS and DLAs measured in Kast spectra, and calibrated with 13 systems that we also observed with HIRES (Burles 1997). These LLS and DLAs were detected as Lyman limits at $2.4 < z < 4.1$. We ignore possible evolution in this mean W_r . We obtained the error by summing three terms in quadrature: 0.2 Å from the calibration, 0.3 Å from the sample size and 0.3 Å for possible bias in the sample. The W_r values have an approximately exponential distribution for small W_r values, with an excess at the largest values from DLAs (Sargent et al. 1980).

Using the values above, we find the contribution to the DA from Ly α lines at $z = 1.9$ in systems with $\log N_{\text{HI}} > 17.2 \text{ cm}^{-2}$ is

$$DA6s = 1.0 \pm 0.4\%, \quad (7)$$

where nearly all of the error is from the uncertain number of LLS at $z = 1.9$. Here, and elsewhere, the suffix “s” refers to a value for $z = 1.900$. Too few LLS are known at redshifts 1.5 – 2.5 to determine how the number per unit redshift changes with redshift.

We checked this result using only the DLAs with $\log N_{\text{HI}} > 20.2 \text{ cm}^{-2}$, or $W_r > 10.3 \text{ \AA}$. The DLAs have $N(z=1.9) = 0.20 \pm 0.04$ from Storrie-Lombardi & Wolfe (2000, Fig. 11), and their mean $W_r = 17.78 \text{ \AA}$, from their Eqn. (3) and Wolfe et al. (1986, Eqn. 3). This mean is for DLAs observed at $1.5 < z < 4$. They have $DA = 0.85 \pm 0.17\%$, where we have ignored the error on the mean W_r . We expect this DA to be smaller than that for all LLS, but the difference is less than we expected. Perhaps the DA6s value is too small. The LLS and DLAs have independent normalization, each has a large statistical error, and we have ignored evolution of the W_r values.

8. Absorption from Metal Lines

To measure absorption by metal lines alone we now introduce

$$DM = 1 - \langle F \rangle, \quad (8)$$

where $F = 1$ if there is no metal line absorption. Since we defined DA to include all types of absorption, $DM \leq DA$ in the DA region. We measured DM in the λ_r range 1225 – 1500 \AA , and we extrapolated to estimate a value for DM in the DA range 1070 – 1170 \AA .

In Figure 10 we show the DM as a function of rest wavelength. We measure DM using the original continuum fits to the Kast spectra, without the corrections for correlations with SNR2 and SDA that we determined for the Ly α forest. Before making this plot we have measured the DM at the same wavelengths in the artificial spectra. Except for continuum level errors, this should be identically zero, since there are no metal lines in the artificial spectra. We saw slight absorption at all wavelengths, showing that we typically place the continuum too high by 0.5% (about 0.15σ per pixel), and we subtracted this from the Kast spectra to give the DM that we show. A straight line fit to these DM values from $1225 < \lambda_r < 1500 \text{ \AA}$ gave:

$$DM1(\lambda_r) = 1.585 - 2.67135 \times 10^{-4}(\lambda_r - 1360)\%, \quad (9)$$

where the λ_r value is in \AA , and DM1 increase slightly as λ_r drops. However, a fit as a function of observed wavelength, λ_o (\AA) gives

$$DM2(\lambda_o) = 1.576 + 9.661 \times 10^{-4}(\lambda_o - 4158)\%, \quad (10)$$

which has a very similar mean near the wavelength, but now DM2 decreases as λ_o decreases. For the Kast spectra in the range 1225 – 1500 \AA the mean $\lambda_o = 4158 \text{\AA}$. We list this and other measurements of the metal absorption in Table 2.

We expect the $DM1(\lambda_r)$ and $DM2(\lambda_o)$ increase with decreasing λ for two reasons: additional lines are included at smaller λ_r , and the density of C IV lines increases at smaller redshifts, or observed wavelengths λ_o . However, the difference in the slopes of DM1 and DM2 indicate that the trend is not strong. Plots of these trends are not too helpful because they are dominated by the huge dispersion in the DM values, which makes it harder to measure the slope of DM with wavelength.

We define $DM3(\lambda)$ as the mean DM in a segment of the spectrum of a QSO that is 121.567 \AA wide in the observed frame, corresponding to $\Delta z = 0.1$ for Ly α . The DM3 values illustrate the huge dispersion in the DM across large parts of a spectrum. We began the first segment for a QSO at 1225 \AA in the rest frame, the next one started where the first one ended, and the last one ended before the minimum of the maximum observed wavelength and 1500 \AA . We ignored the remaining part of each spectrum that gave incomplete segments covering $< 121.567 \text{\AA}$ near the maximum wavelength.

In Figure 11 we show the DM3 values from the Kast spectra as a function of observed wavelength, expressed as redshift for Ly α , to aid comparison with Figure 9. The mean of the DM3 values is $1.87 \pm 0.13 \%$, and the $\sigma(DM3) = 2.5\%$ excluding photon noise, or 2.6% with the photon noise. The distribution of DM3 values is decidedly skew, with a long tail to huge DM3 values. Correlations amongst the DM3 extend right across a spectrum, because absorption systems with high N_{HI} values have many lines, these lines are strong, and they occur all over one spectrum. Moreover, systems are strongly clustered on scales up to 600 km s^{-1} (Sargent et al. 1988).

8.1. Measurement of DM using Line Lists in Published Spectra

We have measured DM4 values using the lists of absorption lines published by Sargent et al. (1988) for 26 QSOs with $1.7 < z_{\text{em}} < 2.3$, excluding Q1510+115 which is BAL. Eleven

of these QSOs are also in our Kast sample. We defined

$$DM4(\lambda) = \sum_{\lambda_i}^{\lambda_i+121.567} W_{obs}/121.567 \text{ \AA}, \quad (11)$$

as an estimator of mean DM from all metal lines in bins of width 121.567 Å in the observed frame. As with the DM3 from the Kast spectra, the first bin started at the maximum of the minimum observed wavelength (Sargent et al. 1988, Table 1) and 1225 Å in the rest frame, and the last bin ended prior to the minimum of the maximum observed wavelength and 1500 Å. Each QSO contributed 4 – 7 segments, and we ignored the partial segments. The mean wavelengths were $\lambda_o = 4125 \text{ \AA}$ and $\lambda_r = 1358 \text{ \AA}$. We took the observed frame equivalent width values W_{obs} from their Table 3. The results, in our Table 2, are similar to those from the Kast spectra: the mean of the 153 DM4 values was $1.67 \pm 0.22 \%$ and the $\sigma(DM4) = 2.74\%$. The mean is nearly identical to that for DM1 from Kast.

DM3 and DM4 differ in several ways. The most obvious difference between the distributions of DM3 and DM4 is that DM4 has a larger fraction of segments with $DM < 0.5\%$, those with few or no absorption lines. The DM3 values are effected by continuum errors, photon noise and weak absorption lines, all three of which are less prominent in the DM4 values. Typical weak lines in Sargent et al. (1988) have $W_{obs} > 0.25\text{\AA}$ that individually give $DM = 0.2\%$. Lines that are weaker than this will have been missed from DM4. The mean values are similar because weak lines do not produce a large part of the total absorption. Given this, the DM4 might have comparable accuracy to the DM3, since the smaller sample for the DM4 will be partly compensated by the lower sensitivity to continuum errors and photon noise.

We have fit the DM4 values as a function of both λ_r and λ_o giving:

$$DM5(\lambda_r) = 1.662 - 5.511 \times 10^{-3}(\lambda_r - 1360)\%, \quad (12)$$

and

$$DM6(\lambda_o) = 1.649 - 7.136 \times 10^{-5}(\lambda_o - 4158)\%. \quad (13)$$

As with the DM1 and DM2 fits to the Kast metal lines, the mean values are similar and the slopes differ. This time the fit to the λ_r has the shallower slope.

8.2. Absorption by C IV

Sargent et al. (1988) and Steidel (1990) found that the number of C IV absorption lines increases as z decreases, and recent measurements show the same trend (Misawa et al. 2002).

We have estimated the DM due to C IV alone using Equation (12) of Sargent et al. (1988). By definition, the total absorption from the stronger of the C IV doublet lines, 1548, is N_*W_* , per unit z . We obtained this by integrating the $n(W_*)$ equivalent width distribution over all W_r , from zero to infinity. This involves an extrapolation to $W_r < 0.15\text{\AA}$ that is probably not much in error because the strong lines that were measured by Sargent et al. (1988) dominate the total absorption. Then

$$DM7(1548, z = 1.957) = N_*W_*(1+z)/1548 = 0.404 \pm 0.074\%, \quad (14)$$

where the $(1+z)$ factor converts W_r to an observed equivalent width, and N_* is the number of lines per unit of z for this line, 1548 Å in the observed frame. We use $W_* = 0.46 \pm 0.04\text{\AA}$ and $N_* = 4.60 \pm 0.74$ for their sample A4, and we assume that the sample is at about the redshift of their sample S2, 1.957. From their Figure 10, at this z the mean $W_r(1548)/W_r(1550) = 1.42 \pm 0.10$ hence,

$$DM7(C\ IV, z = 1.957) = DM(1548) + DM(1550) = 1.704W_r(1548) = 0.69 \pm 0.15\%. \quad (15)$$

The absorption due to C IV increases slightly as wavelength decreases. We make two simple assumptions to measure this trend. First, we scale the $DM7(C\ IV)$ by a factor $[(1+z)/2.957]^\gamma$ where Misawa et al. (2002) find $\gamma = -0.58 \pm 0.46$ for their sample EM15 that includes 136 C IV systems with $W_r(1548) > 0.15\text{\AA}$. Second, we convert the z_{abs} for C IV(1548) to λ_r for Ly α by assuming that all our QSOs are at the mean $z_{\text{em}} = 2.17$: $(1+z_{1548})1548 = \lambda_r(1+z_{\text{em}})$. We find that $DM(C\ IV) = 0.71\%$ at $\lambda_r = 1360\text{\AA}$, which is 0.45 of the total $DM1(1360)$.

8.3. Extrapolating DM into the DA region

At the mean $\lambda_r = 1120\text{\AA}$ where we measure DA, the four extrapolated DM values, DM1, DM2, DM5 and DM6, have a mean of

$$DM1 - 6(1120) = 1.92 \pm 0.42\% \quad (16)$$

where the error is $\sigma/2$.

The DM increases in part because lines with smaller λ_r start to contribute in the spectrum at $\lambda < \lambda_r$. In the range $1225 < \lambda_r < 1500\text{\AA}$ these include Si IV 1394, C II 1334, O I 1302, Si II 1260 and N V 1229. In the wavelength range 1070 – 1170 Å such lines include Si II 1193 and especially Si III 1206.

We increase our estimate of the DM in the Ly α forest by a factor of 1.2 ± 0.1 to account for the increasing number of lines as a function of decreasing λ_r because we suspect that

these lines are not adequately accounted for by the trends with λ_r . The adjustment has a large error because it is based on our examination of only 9 spectra of high resolution at these redshifts.

The DM we will use is then

$$DM_s(\lambda_r = 1120) = 2.3 \pm 0.5\%, \quad (17)$$

We estimated that had we been able to measure DMs values, in the Ly α forest, in bins of $\Delta z = 0.1$, those values would have $\sigma = 3.1\%$, which we obtain from $\sigma \propto (\text{mean DM})$, using $\sigma(DM3) = 2.5\%$ for mean DM3 = 1.87%.

We find that the metals account for $15 \pm 4\%$ of the total DA at $z = 1.9$. This is less than the estimate of Rauch et al. (1997), from a few QSOs, that about 22% of the total DA is from metals at $z \simeq 2$. If Rauch et al. (1997) used a path length of about $\Delta z = 0.9$ from about 3 QSOs, then their DM would have a relative error of order $3.1/(2.3 \times \sqrt{9}) = 0.45\%$, sufficient that the difference from our estimate would not be significant.

9. Dispersion of DA Values

We have long known that there is a lot of scatter in the amount of Ly α forest absorption present in different low z_{em} QSOs: Carswell et al. (1982, §7), Tytler (1987), Kim et al. (2001, Fig. 15), and Kim et al. (2002, Fig. 8). Schaye et al. (2003) found that the χ^2 per degree of freedom of DA measured in intervals of about $\Delta z = 0.2$ was 5.2 when they use all DA absorption, and remained 2.4 after they had removed metal lines and DLAs. They stated that this residual scatter was probably cosmic variance.

We now measure the dispersion of DA values measured in segments of spectra of length $\Delta z = 0.1$, and we estimate the individual contributions of the low density IGM, the Ly α lines of LLS and the metal lines.

9.1. DA2: The Mean DA in $\Delta z = 0.1$ Intervals

We have already displayed the standard deviation of the pixel values of DA, $\sigma(DA0)$, on various Figures, and we saw that the values were large and similar in size to the mean DA values. A significant part of the $\sigma(DA0)$ values is from the photon noise. However, had we removed the photon noise, the $\sigma(DA0)$ values would be smaller than the standard deviation of the true flux from the QSOs, because the Kast spectra do not resolve spectra lines. The

Kast spectrograph makes absorption lines shallower.

We have examined the dispersion in the DA values using segments of spectrum of length $\Delta z = 0.1$, which is 121.567 Å in the observed frame or 108 Kast pixels. The velocity interval from one end of a segment to the other is 10335 km s⁻¹ (Sargent et al. 1980, Eqn. 20), and in a model with $H_o = 71$ km s⁻¹ Mpc⁻¹, $\Omega_\Lambda = 0.73$, and $\Omega_m = 0.27$, $\Delta z = 0.1$ centered at $z = 1.9$ is 152.57 comoving Mpc.

We define a DA2 value as the mean DA in a segment of the spectrum of one QSO that is 121.567 Å long.

In Figure 12 we show the DA2 values from the Kast spectra. We started at the lowest z covered by each spectrum, and made points for each 0.1 segment, discarding the remainder of length < 0.1 at the high z end. This explains why there are many dark (blue) points at the lowest redshifts and few at the highest redshifts. We then added light (red) points for bins starting at z values larger by 0.05, to better show the high redshifts and the DLAs. Many pixels then contribute to two points on the plot. We also show the DA(z) curve from Figure 9.

The contribution of photon noise to the $\sigma(DA2s)$ values is small, except for a few segments. The $\sigma(DA2s)$ from photon noise alone in a 108 pixel segment is 0.96% for S/N = 10 per pixel, rising to 3.8% by S/N = 5. The few segments with S/N < 5 are all in the lowest z_{abs} bin in Figure 12, and they alone have $\sigma(DA2s) = 0.08$, while the remaining segments have the $\sigma(DA2s) = 0.06$. The same applies to the equivalent point on Figure 9.

Figure 12 shows that the distribution is asymmetric, with a small fraction of segments having unusually large DA2 values. Due to the accidents of the bin placement, 3 additional high points, all due to DLAs, are seen in the shifted bins (red). These DLAs are present in the blue sample as well, but due to an accident of bin placement their DA is split between two bins. The dispersion of the (blue) points about the mean DA(z) (not the curve) is 6.81%, about half of the mean DA due to Ly α alone.

To remove the portion of the dispersion in DA that is due to the z trend, we define DA2s, where the suffix “s” refers to values scaled to the values we expect at $z = 1.900$ using the DA(z) trend from Equation 5.

9.2. Comparison of DA2s in Kast and Artificial Spectra

In Figures 13 and Figure 14 we show the distribution of DA2s in the Kast and the artificial spectra. We list parameters of the distributions in rows 1 and 6 of Table 3. We

have not adjusted the artificial spectra to exactly match the absorption in Kast spectra, especially at this low z , and hence any agreement is accidental. We see that the two have similar mean DA2s, however the Kast have a larger dispersion, as we might expect because they contain Ly α lines from LLS and metal lines. For example, the Kast spectra include three very high DA values, all from DLAs, that do not show on Figure 13. In row 2 of Table 3 we also give statistics for just the segments with DA2s < 0.35 . Both the mean and the standard deviation are reduced as we would expect, but the $\sigma(\text{DA2s})$ for the Kast segments remains larger (about 3σ level) than that for the artificial segments.

The approximate similarity of the artificial and Kast spectra means that the artificial spectra were well suited to help us find and remove the biases in the continuum fits. The artificial spectra accidentally contained about the correct total amount of absorption, although they were designed to model just the low density IGM. If we were attempting to make the artificial spectra very similar to the Kast ones, they should have less absorption from the IGM, and they should include contributions from LLS and metals.

9.3. Calculation of the dispersion in the DA from the IGM

We can calculate the expected variation in the amount of absorption in a spectrum. We restrict the calculation to the absorption from the Ly α lines in the lower density portions of the IGM. We ignore absorption by the Ly α lines of LLS and metal lines. We shall introduce the notation

$$\sigma(\Delta z) = \sigma(\text{DA2s low density IGM only}) \quad (18)$$

for the standard deviation of the mean DA in spectral segments of length $\Delta z = 0.1$. The $\sigma(\Delta z = 0.1)$ values are the 1D flux analogues of the 3D mass σ_8 values, (Kolb & Turner 1990, Eqn 9.18, Fig 9.2). The $\sigma(\Delta z = 0.1)$ value is of great interest because it is a measure of the power in flux in the Ly α forest on scales of 153 Mpc, and it is related to the mass power spectrum.

McDonald (2003, Fig. 10a) shows that the relationship between the 3D matter and flux power depend on scale. On large scales the flux power is proportional to the matter power, and hence to σ_8^2 . On small scales an increase in the matter power leads to larger velocities that smooth the fluctuations in the flux, and decrease the flux power. At a scale of $k \simeq 0.013$ (s/km) (1.5 Mpc) the flux power is insensitive to the mass power.

We can derive the variance of the DA2 values by integrating the power spectrum of the flux over a top hat window function of width $\Delta z = 0.1$.

First of all, we generate one dimensional flux power spectrum, $P_{F1D}(k)$, by following the

McDonald (2003) parameterization. We introduce $\delta A_1 = 0.218$ to adjust the cosmological parameters and redshift, and $\delta \overline{F} = 0.0419$ to match the mean flux with our measured value (McDonald 2003, Table 1). Then we calculate,

$$\sigma(\Delta z = 0.1)^2 = \langle F \rangle^2 \int P_{F1D}(k) W^2(k) dk \quad (19)$$

where $W(kR)$ is the top hat window function. We correct the result to our definitions of flux, since in our units McDonald (2003) uses $(F - \langle F \rangle) / \langle F \rangle$, a flux deviation divided by the global mean flux at that z . For one dimensional case, we have

$$W^2(kR) = \frac{2(1 - \cos(kR))}{(kR)^2} \quad (20)$$

where $R = 10335 \text{ km s}^{-1}$ for $\Delta z = 0.1$.

We obtain $\sigma(\Delta z = 0.1) = 0.057$ at $z = 1.9$ with $DA = 0.118$ and $\sigma_8 = 0.9$, for the low density IGM alone.

9.4. Measurement of the dispersion in the DA from the IGM

A measurement of $\sigma(\Delta z = 0.1)$ has several uses. It provides a check on the linear model bias parameters b'_δ and β (McDonald 2003). The scale of $\sigma(\Delta z = 0.1)$ is large enough that we are well in the linear regime, and the astrophysical complications such as fluctuations in the thermal history and temperature and UVB will be less important than on small scales. If we know the bias parameters from calculations, we can calculate a normalization for the mass power spectrum that is a larger scale and earlier epoch analogue of σ_8 .

The $\sigma(\Delta z = 0.1)$ value is hard to measure because we must estimate and subtract the portion of the dispersion coming from the Ly α lines in LLS, metal lines and continuum fit errors.

In Table 3 we list the mean and σ of the DA2 values for the Ly α lines of LLS (including DLAs). We calculate that $\sigma(DA2)$ for the Ly α of LLS is 0.035 by randomly sampling their W_r values. We have checked this result analytically. Since the expected number of LLS per $\Delta z = 0.1$ is only 0.14, 0.869 of segments have none, 0.122 have one, and 0.009 have two or more, if we ignore clustering. We then obtain the approximate σ of the DA of the Ly α of the LLS from the sum of the squares of the W_r values. In Table 3 we also list the equivalent values for the metal lines alone, mean DM2 and its σ taken from the end of §8.

Both the Ly α of LLS and the metal lines have a much larger effect on the $\sigma(DA2)$ values than they do on the mean DA2 values. The standard deviations of the amount of absorption

from the Ly α of LLS, $\sigma(DA2)$, is about 3.4 times the mean value. Similarly, the metal line $\sigma(DA2)$ is 1.3 times the mean. Both distributions have long tails with huge values. The two distributions are more asymmetric than either Poisson or exponential distributions, both of which have σ equal to their means.

We estimated the σ of the DA2s of the Ly α in the IGM alone, $\sigma(\Delta z = 0.1)$ by adding random contributions from the IGM, LLS and metals. We assume that the DA2 values for the Ly α forest alone are drawn from a Normal distribution with mean 11.8% and the one free parameter, the unknown $\sigma(\Delta z = 0.1)$. We made mock DA2 values by adding together three random numbers:

- DA2 from the Ly α forest alone: A random deviate from the Normal distribution.
- DA2 from the LLS: A randomly selected DA2 value drawn from the known distribution of W_r values for LLS (including DLAs).
- DM2 from the metals: A randomly selected DM2 value, scaled to 1120 Å.

The mean DA2 for these mock spectra does not change as we vary the $\sigma(\Delta z = 0.1)$ value. We found that the mean DA2 from the mock spectra was 0.151, about 1σ lower than the mean DA2s that we give in Table 3, and identical within the errors to the value in Table 4, as expected, since we are using the same data. We estimate a 68% confidence interval of $0.032 < \sigma(\Delta z = 0.1) < 0.044$, with a best value of 0.039. For these values, the mock segments matched the observed $\sigma(DA2s) = 0.0612 \pm 0.0035$.

The values we give for $\sigma(\Delta z = 0.1)$ may have a larger error than we have estimated, because the many factors that contribute to the measurement are not well known. The dispersions from the metals involves an extrapolation, and we have assumed that the contribution from the continuum error is insignificant.

The $\sigma(\Delta z = 0.1)$ value includes the dispersion from both the Ly α in the low density IGM and the continuum errors, because we did not include the latter in three part model for the mock segments. The dispersion of the DA in the artificial spectra, without noise or continua fits, was 0.0441. When we re-measured this dispersion after adding photon noise and fitting the continua we found 0.0422, from Table 3, which shows no significant increase from the fits. This implies that the continuum fits have an insignificant error. Below we will see that the dispersion from a hydrodynamic simulation suggests that our $\sigma(\Delta z = 0.1)$ value is approximately correct, and hence that the continuum error is not a major part of the value. However, if we treat the continuum fits as absorbed spectra, the dispersion of the equivalent DA is 0.0325, which suggests that the continuum error is a significant part of the

$\sigma(\Delta z = 0.1)$ value. We intend to investigate this issue in future work starting with a fully automated continuum fitting algorithm that should be more stable.

The Ly α absorption from the low density IGM, the Ly α from LLS and the metal lines all appear to contribute similar amounts to the dispersion in the DA2s values in $\Delta z = 0.1$ bins at $z = 1.9$. Kim et al. (2004, Fig. 3) showed that metal lines comprise a large part of the power on small scales ($k > 0.05$ s/km), but only 0.07 of the total power on scales $\simeq 100$ km s $^{-1}$. Since integrated power is proportional to variance, this implies that the metals will contribute about 7% of the variance on scales of 100 km s $^{-1}$, which is only 1% of the 10,335 km s $^{-1}$ span of $\Delta z = 0.1$. We find that the metals comprise $(0.031/0.0612)^2 = 0.26$ of the total variance sampled in bins with $\Delta z = 0.1$. On these large scales the dispersion due to the metals becomes a larger part of the total because the absorption by metal ions is strongly correlated across these large scales. A single absorption system can put strong metal lines all over a spectrum. The correlation arises from the multiplicity of strong spectral lines, and not from the distribution of matter on 153 Mpc scales.

Our $\sigma(\Delta z = 0.1)$ value may be too large because we ignored the correlation of LLS and metal lines. The absorption systems that show many strong metal lines are likely to be LLS. The DLAs in particular also have a lot of metal lines, especially when the gas covers a wide range of velocities, and the metal abundances are high. Hence the mock spectra that we made to calculate $\sigma(\Delta z = 0.1)$ would be more realistic if the we had chosen a large DM2 value, rather than a random one, whenever a segment had a Ly α with a large W_r value. This correction would make more segments with very large DA2 values, which would increase the variance from the metals and LLS, and hence decrease our estimate of the $\sigma(\Delta z = 0.1)$. We have not modeled this complication, because the metal lines lie at specific velocities relative to the Ly α line and we should make complete mock spectra, with realistic mock absorption systems. Alternatively, and preferably, we could use spectra of high spectral resolution and remove the metal lines and the Ly α of the LLS.

We have no good explanation of why the $\sigma(\Delta z = 0.1)$ value that we measured, $0.039^{+0.005}_{-0.007}$ is 3.6σ less than the value we calculated. Measurement error is a clear option, especially since this is the first ever such measurement. However, systematic effects from the photon noise, continuum fit and LLS – metal correlations should all have lead our measured value too be large, not too small, and to obtain a $\sigma(\Delta z = 0.1) = 0.057$, we would have to have greatly overestimated the σ from both the metals and the LLS. The calculation is also uncertain and untested and involves various uncertain scalings.

10. DA3: The DA in Quarters of the Sample

To obtain an accurate mean DA value we need to average over a substantial path length, from many lines of sight, because the distribution of DA is not normal. If the DA0 values were normal deviates we would expect that the standard deviations of the DA2s points would be about 10 times smaller than that of the DA per pixel, DA0, because there are about 108 pixels per DA2 point. However $\sigma(\text{DA2s})=6.12\%$, only 3 times less than $\sigma(\text{DA0s}) = 20.3\%$. When we average from 1 to 100 pixels the DA0 distribution is asymmetric because the Ly α forest at $z = 1.9$ is largely absorption free, with well separated lines making most of the absorption. Bernardi et al. (2003, Appendix C) discuss another consequence of this asymmetry.

We have explored the dispersion of the mean DA in much larger bins. We divided the spectra, both artificial and Kast, into four groups, or quarters, giving the DA3s values that we list in Table 4. We used Equation (4) to scale these values to the expected value at $z = 1.9$, because the fourth quarter happened to have a significantly lower mean z . We assigned the QSOs to quarters in RA order, to emphasize a possible source of bias. QSOs with similar RA values are more likely to be observed at the same time, through similar conditions, giving more similar S/N, and to have their spectra reduced in the same way. Our initial continuum fits were also done in RA order, although later adjustments were done in order of emission line strength, and S/N. The RA order of the artificial spectra is that of their partner QSOs.

The first column is the DA3s in the input artificial spectra, with flux range 0 – 1, plus photon noise. If the simulations were a faithful representation of the IGM absorption, the error on the mean of these values, $\sigma(\mu) = \sigma/2 = 0.48\%$ would be an estimate of the portion of the error in the DA from the 77 Kast spectra due to the sample size. From an examination of a much larger sample of similar artificial spectra, we calculate an expected $\sigma(\mu) = 0.4 - 0.5\%$ for a sample at $z = 1.9$ with a path length of 19.75.

This is the error we would have obtained had our spectra been perfect, and the continuum fits perfect. However, the artificial spectra have more absorption than the low density IGM alone, and they lack high N_{HI} lines and metal lines. Hence the error for the Kast spectra will be somewhat larger.

The second column shows our measurements of the DA3s in the artificial spectra with emission lines and S/N like our Kast spectra. The dispersion in this column will include many effects, especially the continuum level errors and our corrections for the biases that we measured as a function of SNR2 and SDA. The mean of this column is nearly identical to the equivalent values in the first column because the corrections that we made to the continua

forced agreement. The σ values are similar because the continuum fits did not increase the dispersion.

The third column shows the row by row difference between the DA3s values in the first two columns: the four true DA3s values, minus our measurement of each. The dispersion in this column is the portion of the measurement error coming from the S/N, and especially our continuum fitting and continuum level corrections. The error on the mean of $\sigma(\mu) = 0.32\%$ is again less than the error in the first column, 0.48%. This implies that our spectra, their S/N, our continuum fits, and our corrections to the continuum fits are adequate for a sample of 77 QSOs at $z = 2$.

The fourth column shows the DA3s values for the quarters of the Kast QSO spectra. The error on the mean is the largest of the values for the different columns, as expected, because we are now sensitive to the large N_{HI} lines and metal lines. We already saw working with the DA2s $\Delta z = 0.1$ values that the metal lines and the $\text{Ly}\alpha$ of LLS have a large effect.

11. Error on Our DA Measurement

The 1σ error terms associated with our DA4 estimate are:

- 0.64% estimated from the dispersion in quarters of our sample (Table 4, column 5). This includes sample variance and that part of the calibration error that varies between the quarters.
- 0.32% calibration error, from Table 4 column 4. Estimate of the error in the corrections that we applied to the continuum levels that correlated with SNR2 and SDA.
- 0.48% sample variance, from the size of our sample, (sometimes called cosmic variance).
- 0.6% uncertainty in the amount of metal absorption
- 0.4% uncertainty in the amount of absorption from $\text{Ly}\alpha$ lines with $\log N_{\text{HI}} > 17.2 \text{ cm}^{-2}$.

To obtain DA4s, we first scaled the DA0 values for each pixel to the expected value at $z = 1.9$, using Equation (4), before taking the mean. The result is slightly different from a scaling of the mean DA4, using the single mean z_{abs} value. As our estimate of the error on our DA4s measurement we use the quadratic sum of the errors on the first two terms above, giving

$$DA4s(z = 1.9) = 15.1 \pm 0.7\%, \quad (21)$$

where the suffix “s” means that the value applies to $z = 1.900$.

For comparison with measurements or simulations that do not include metal lines, we can subtract $DMs = 2.3 \pm 0.5\%$ for the metal lines, giving $DA7s = DA4s - DMs$, or

$$DA7s(z = 1.900) = 12.8 \pm 0.9\%, \quad (22)$$

and for comparison with data or simulations that include neither metal lines nor Ly α lines from systems with $\log N_{\text{HI}} > 17.2 \text{ cm}^{-2}$ (all LLS and DLAs) the appropriate DA is $DA8s = DA4s - DA6s - DMs$, or

$$DA8s(z = 1.900) = 11.8 \pm 1.0\%. \quad (23)$$

12. Comparison with Hydrodynamic Simulations

In this section we will compare the DA from the Kast spectra to values from full hydrodynamic numerical simulations. We will give a more thorough description in Jena *et al.* 2004.

We used the cosmological simulation code, ENZO (Norman & Bryan 1999), which follows both dark matter dynamics and hydrodynamics consistently. The collisionless dark matter particles are evolved using a Lagrangian particle-mesh method whereas the equations of gas dynamics are solved using a piecewise parabolic (PPM) method.

The simulations assume an evolving UV background radiation field due to both quasar and stellar sources as described by Madau *et al.* (1999). From this spectrum we calculate photo-ionization and photo-heating rates for H I, He I, and He II assuming the gas is optically thin. Although we believe that we have the appropriate level of ionization in the low density IGM, the gas remains optically thin in the simulation even in high density regions, and hence we over ionized the densest regions and the spectra do not include any LLS or DLAs. The highest column density in any of the artificial spectra that we made was $\log N_{\text{HI}} < 17 \text{ cm}^{-2}$. To account for the extra heating from late He II reionization due to opacity effects (Abel & Haehnelt 1999), we multiply the He II photo-heating rate by $\gamma_{228} = 1.8$. Bryan & Machacek (2000) have shown that this level of heating is needed to match the b -parameter distribution of the Ly α forest. This is equivalent to $\gamma_{228} \simeq 2.4$ in simulations with higher resolution.

We used a spatially flat Λ CDM universe with $\Omega_b = 0.044$, $\Omega_m = 0.27$ and $\Omega_\Lambda = 0.73$. We used $H_0 = 71 \text{ km s}^{-1} \text{ Mpc}^{-1}$ an initial power spectrum index $n = 1.00$ and we normalized the power spectrum to $\sigma_8 = 0.9$. These values are similar to the best fit values using the WMAP first year data (Spergel *et al.* 2003), but we chose a slightly larger σ_8 consistent with other measurements.

We ran the simulation with a box size of $54.528h^{-1}$ Mpc, or 75.7 comoving Mpc with a grid size of 1024^3 . This provides us with enough resolution and included the effects of some of the larger scale power missing from smaller boxes. The initial perturbations were assumed to arise from a Harrison-Zel’dovich power spectrum with a CDM transfer function. These density perturbations were then converted to initial velocities using the Zel’dovich approximation. The simulation was run on the Blue Horizon computer at the San Diego Supercomputing Center.

We make several points about the comparison of the hydrodynamic simulation and the Kast spectra.

First, we should compare the simulated spectra to the DA values for the IGM only, without metal line or the Ly α of LLS.

Second, although the DA in a single DA2s segment will differ from the mean in the universe, by design the mean DA in the simulation box should be the mean in the universe for the physics and parameters that were simulated.

Third, the 150 simulated spectrum segments were all made by passing lines of sight through the same 76 Mpc volume. To obtain one segment, the line of sight traveled about two times through the box. Their dispersion is reduced because the same modes, both short and especially long ones, are sampled many times.

Lastly, the simulation was made in a 76 Mpc box that contained no power on scales ≥ 38 Mpc, and reduced power on somewhat smaller scales because the boundary conditions were periodic.

We list the results from the spectral segments of length $\Delta z = 0.1$ from the hydrodynamic simulation in row 7 of Table 3, along with the other comparable measures of the DA2s. In Figure 15 we show the distribution of DA2s from the hydrodynamic simulation. The mean $DA2s = 12.87 \pm 0.27\%$ is 1.08 ± 0.09 times that for the Kast IGM only from Table 3. The simulation had slightly too much absorption. The $\sigma(\text{DA2s})$ of the simulated spectra was 0.85 ± 0.14 times the $\sigma(\Delta z = 0.1)$ from the Kast IGM only, slightly too small. We expect the simulations to have the same mean and a smaller σ than the Kast IGM only values.

There are three obvious ways to adjust the parameters of the simulation to better match the DA of the Kast spectra. We could increase the UVB intensity, which reduces the amount of H I. We could reduce the $\Omega_b h^2$ which has the same effect, or we could increase the σ_8 which removes baryons from the low density IGM where they absorb most.

In Figure 16 we show the approximate intensity of the UVB required to explain the mean DA at $z = 1.9$. The vertical axis Γ is the photo-ionization rate per H I atom in the low

density optically thin IGM. We use the units of the predicted rate at $z = 1.9$ from (Madau et al. 1999):

$$\Gamma = 1.329 \times 10^{-12} \gamma_{912} \text{ s}^{-1}, \quad (24)$$

where γ_{912} is a dimensionless number. Madau et al. (1999) predicted $\gamma_{912} = 1$, and when we adopt their spectrum shape, the ionization rate is proportional to the intensity of the UVB, J . We show how the UVB intensity required to give the $DA8s = 0.118 \pm 0.010$ for the Kast IGM only as a function of σ_8 . We found these curves using scaling relationships that we derived from many simulations that we ran with a variety of parameters in boxes four times smaller. A smaller intensity is required when we have a larger σ_8 , since there are then fewer baryons in the IGM that we need to ionize.

The changes required in any one of the three parameters to match the observed DA are modest. In Table 5 we list these changes. In the first row we give published estimates for Ω_b and σ_8 from Spergel et al. (2003), γ_{912} from Madau et al. (1999), and DA8s from this paper. The simulations shows that these values are not quite concordant. We will discuss γ_{228} elsewhere, since high resolution spectra are needed to assess the changes it makes to the widths of Ly α forest lines. In the second row we give the DA from the simulation, which differs from the Kast value. The third and fourth rows show the σ_8 and γ_{912} values from Figure 16. We obtain the Ω_b estimate in the fifth row using

$$\Omega_b = 0.044(\tau_{eff}/0.1378)^{1/\alpha} \quad (25)$$

from Equation 1, where $\tau_{eff} = 0.1378$ corresponds to the $DA(z=1.9) = 12.87\%$ from the simulations with $\Omega_b = 0.044$, and we use $\alpha = 1.7$. The values in rows 2 – 5 give alternative concordant models for the IGM.

The errors that we quote in rows 3 – 5 of Table 5, for γ_{912} , σ_8 and Ω_b are from the DA8s error alone, assuming that all other parameters are known without error, and that the simulation is an accurate representation of the IGM. These errors are as small or smaller than those usually quoted for these parameters, which shows that the accuracy that we have obtained for DA is sufficient to give new cosmological information. For example, if the σ_8 and γ_{912} values had insignificant errors, the $\Omega_b = 0.0417 \pm 0.0022$ from our DA measurement would be more accurate than that using our measurements of D/H: $\Omega_b = 0.042 \pm 0.004$ (Kirkman et al. 2003), and comparable in accuracy to that from the first year WMAP data, $\Omega_b = 0.0444 \pm 0.0018$ (Spergel et al. 2003).

Our DA value gives γ_{912} to higher accuracy than has been possible before. In the last row of Table 5 we give $\gamma_{912} = 1.08 \pm 0.27$ or $\Gamma = (1.44 \pm 0.36) \times 10^{-12} \text{ s}^{-1}$, where the error now includes the contributions from the errors on the other three parameters that we list. The main contribution to this error is from the uncertainty in σ_8 . We illustrated this in Figure 16.

The DA value alone leaves a strong degeneracy between the best fit UVB intensity and σ_8 values. We can break this degeneracy using the variation in the DA, from the power spectrum of the flux, or from $\sigma(\Delta z = 0.1)$ if we know the linear bias for the appropriate model.

If we change the parameters to reduce mean DA, the $\sigma(\text{DA2s})$ will also decrease, and it is already smaller than the Kast IGM value. However, we expect the simulation $\sigma(\text{DA2s})$ to be smaller than the Kast, because of the finite size of the simulation box, and it is beyond the scope of this paper to determine whether the reduced value would be compatible with the spectra. However, we did check that the power of the flux in these lines of sight does approximately match that in HIRES spectra on much smaller scales, $0.008 < \log k < 0.08$ (s/km) at these redshifts.

13. Sample Size, Spectral Resolution, LLS and Metals

The asymmetric DA distribution extends to scales > 153 Mpc. There remain correlations in the Ly α absorption from the IGM, from the matter power spectrum on large scales. The metal lines are correlated because one system can create lines all over a spectrum. The DA distribution is also asymmetric because the Ly α lines of LLS and DLAs are rare events that produce huge DA values. When we take the mean of 152 DA2s values from Table 3, we would expect the $\sigma = 0.0612/\sqrt{152} = 0.50\%$ if the DA2s were uncorrelated and normally distributed. Instead we find $\sigma(\text{DA3s}) = 0.64\%$, from Table 4. The σ decrease more slowly than $(\Delta z)^{-0.5}$.

To help us compare measurements from different samples, we can use a first order estimate

$$\sigma(\text{DA}s, z = 1.9) = 0.024(\Delta z)^{-0.4}, \quad (26)$$

where Δz is the path length in the sample at $z = 1.9$, and the coefficient and power are from a straight line fit to the $\sigma(\text{DA3s})$ from the quarters of the Kast the sample (Table 4) and $\sigma(\text{DA2s})$ from the $\Delta z = 0.1$ (Table 3). This σ is for DA values that include metal lines and the Ly α of LLS. Each QSO contributes a maximum of $\Delta z = 0.156(1 + z_{em})$ when we use all wavelengths from Ly β to Ly α , and, for our sample, typically around 0.6 of this or $\Delta z = 0.3$ at $z = 1.9$.

We expect to obtain approximately the same $\sigma(\text{DA})$ with four times smaller Δz when we use spectra that are free of both the metal lines and the Ly α from LLS. Our estimate that the $\sigma(\text{DA2s}) = 0.039 \pm 0.006$ implies that we might achieve

$$\sigma(\text{DA}) = 0.012(\Delta z)^{-0.5}, \quad (27)$$

with such spectra. This suggests that we might obtain an error on DA8s (IGM only) of 1% with only 5 high resolution spectra, comparable to the error we obtained with the 77 Kast spectra, after we removed the mean absorption by LLS and metal lines. However, we would need improvements in the flux calibration and continuum fitting to echelle spectra to obtain errors in DA of 1%. Suzuki et al. (2003) found it very difficult to obtain such small errors, using purpose built software, and with ample calibration spectra.

14. Comparison with Prior Measurements

The few prior estimates of DA at $z = 1.9$ all involve small samples and they are all compatible with our new measurements.

Kim et al. (2001, Figure 15) show measurement from about 11 QSOs near that z , with a mean DA of about 10% and a range of 6% – 15% that includes the values from the Kast spectra. They fit a power law to τ_{eff} values from UVES and HIRES spectra, some of which include systems with high N_{HI} lines, but no metals, giving $\text{DA} = 10.9$ at $z = 1.9$. Our equivalent value, between the values for DA7s and DA8s, is approximately 12%.

Rauch et al. (1997) measured DA in 7 HIRES spectra. They identified and rejected metals and all lines with $b < 10 \text{ km s}^{-1}$. At $z = 2.0$ they found DA 14.8%, with no error offered. Since only two QSOs contributed data at $z < 2.3$, we estimate their error is $> 1.6\%$ (Equation 27). Our equivalent value, $\text{DA7s} = 12.8 \pm 0.9\%$, is smaller.

Schaye et al. (2003) present a measurements of DA from high resolution UVES and HIRES spectra of 19 QSOs, with 6.6 km s^{-1} resolution, 8 of which contribute at $z = 1.9$. Their best fit (Fig. 1) give $\text{DA}(1.905) = 12.6\%$, or 10.9 after they remove metal lines and $\text{Ly}\alpha$ lines from systems with $\log N_{\text{HI}} > 19 \text{ cm}^{-2}$. Our equivalent value is approximately $12 \pm 1\%$, and it is larger, but not significantly.

Meiksin & White (2004) looked the apparent discrepancies in the estimates of the average $\text{Ly}\alpha$ absorbed flux for $z > 2.4$, and found that when the results were interpreted on a consistent statistical basis, all the estimates roughly agreed. They find $\text{DA} = 0.18 \pm 0.002$ at $z = 2.41$, which is basically consistent with the value that we would infer at the same redshift (Figure 12).

15. Discussion and Summary

We have measured the amount of absorption in the Ly α forest in spectra of 77 QSOs from the Kast spectrograph on the Lick 3m telescope. We measured the mean amount of absorption and the contributions from the Ly α lines of LLS and metal lines. We also measured the variance in the amount of absorption from the metals, the LLS and the Ly α in the lower density IGM. The amount of absorption that we find is consistent with that in a large hydrodynamic simulation that uses popular values for the cosmological and astrophysical parameters. We summarize this work under these three topics, and the opportunities for improvements.

15.1. Mean DA

We fit continua to the Kast spectra, and to artificial spectra that we made to mimic them. The relative error in our continuum fits to the artificial spectra is 3.5% on average. The mean error for all 77 spectra is within 1–2% of the correct value, except when the S/N per 1.13 Å pixel is < 6 where we systematically placed the continuum too high. We corrected this systematic bias and also our tendency to place the continuum 0.5% too high where there is a lot of absorption.

We find that the total absorption in the Ly α forest between 1070 and 1170 Å at $z = 1.9$ is $DA = 15.1 \pm 0.7\%$, including absorption by metal lines and the Ly α lines of LLS (defined to include all DLAs). This is the first measurement of DA to be made at any z using a calibrated continuum fitting procedure, and the first of any sort using a large sample at $z \simeq 2$.

We measured the mean absorption due to metals at 1225 – 1500 Å in both our 77 Kast spectra and from the lists of absorption lines in 26 spectra in Sargent et al. (1988). The results agree. Near $\lambda_r = 1360$ Å $DM3 = 1.87 \pm 0.13 \%$ from our Kast spectra and $DM4 = 1.67 \pm 0.22 \%$ from Sargent et al. (1988).

We must extrapolate the DM to obtain the metal absorption in the Ly α forest and this increases the uncertainty. The extrapolation gives $DM1 - 6(1120) = 1.92 \pm 0.42\%$, and we increase this by a factor of 1.2 to account for extra metal lines in the Ly α forest, giving $DMs = 2.3 \pm 0.5\%$.

The total absorption in rest wavelengths 1070 – 1170 Å comprises: $DA6s = 1.0 \pm 0.4\%$ from LLS, $DMs = 2.3 \pm 0.5\%$ from metals and $DMA8s = 11.8 \pm 1.0\%$ from the Ly α in the low density IGM that excludes Ly α lines with $N_{\text{HI}} > 17.2 \text{ cm}^{-2}$.

The absorption from metals is important. At $z = 1.9$ the metals are $15 \pm 4\%$ of the total absorption, and $19 \pm 5\%$ of the absorption by just the Ly α with $\log N_{\text{HI}} < 17.2 \text{ cm}^{-2}$. We have calculated the amount of absorption due to C IV alone, which increases slowly as z_{abs} drops, and hence λ_r for a given QSO sample. By $\lambda_r = 1120 \text{ \AA}$ at $z = 1.9$ C IV gives $\text{DM7} = 0.80\%$ that is 35% of the metal line absorption.

We calculated the absorption by the Ly α lines of LLS, using a list of rest equivalent widths from other Kast spectra, and normalizing to the LLS density seen in HST spectra. We find $\text{DA6s} = 1.0 \pm 0.4\%$, where the error is nearly all from the uncertain density of LLS at these low redshifts and the suffix “s” refers to a value for $z = 1.9$. We calculated that the DLAs alone have $\text{DA} = 0.85 \pm 0.17\%$, which is a larger proportion of the DA6s for all LLS than we expected. Perhaps the DA6s value is too small.

15.2. Dispersion of DA values

We have measured the dispersion in the mean DA on large scales. We defined DA2s to be the mean DM in segments of a spectrum of length $\Delta z = 0.1$, or 121.567 \AA in the observed frame. This is 153 comoving Mpc at $z=1.9$. We scale the measurements to the amount of absorption expected at $z = 1.9$ since the evolution is significant. We find $\sigma(\text{DA2s}) = 6.12 \pm 0.35\%$. This is a measure of the amount of power in the flux distribution on scales similar to 153 Mpc, however it includes the power due to the Ly α of LLS and the metal lines, and the power in the error in the continuum fits.

We have estimated the dispersion in the DA2s from the Ly α lines of LLS by making mock spectral segments of length $\Delta z = 0.1$. We added random samples of measured W_r values to the segments. We find $\sigma(\text{DA2s}, \text{LLS}) = 3.5 \pm 0.5\%$, much larger than the mean value of $1.0 \pm 0.4\%$. We also derived this σ analytically.

We have measured the dispersion in the amount of metal absorption in the Kast spectra: $\sigma(\text{DM3}) = 2.5\%$. We found a similar value from the Sargent et al. (1988) spectra: $\sigma(\text{DM4}) = 2.7\%$. These are the measured standard deviations of the DM values in spectral segments of $\Delta z = 0.1$, at $z = 1.9$ and $\lambda_r = 1360 \text{ \AA}$, which is near $\lambda_o = 4130 \text{ \AA}$.

We have estimated the dispersion that we expect from the metal lines in the Ly α forest. We scale from $\sigma(\text{DM3}, \lambda_r = 1360) = 2.5\%$, to obtain $\sigma(\text{DMs}) = 3.1\%$. Since this value is from an extrapolation, its error is large and not well known. It appears to be larger than the mean DMs, $2.3 \pm 0.6\%$.

We calculated the dispersion of mean DA in segments of spectra 121.567 \AA long, from

the absorption in the low density IGM alone, is $\sigma(\Delta z = 0.1) = 3.9_{-0.7}^{+0.5}\%$. This value includes the dispersion from the error in continuum fits which is probably small. We are able to detect the power on large scales because the Kast spectra and the continua that we fit are more stable over these large scales than are high resolution echelle spectra and their continua (Suzuki et al. 2003). The $\sigma(\Delta z = 0.1)$ that we measure is larger than a value we calculated, for no clear reason. Both the measurement and calculation could have large errors.

The dispersion of DA measured in segments of spectra 121.567 Å long in the observed frame at $z = 1.9$ for Ly α comes about equally from the low density IGM, LLS and metal lines.

The flux field is significantly different from a random Gaussian field, with an enhanced probability of a large amount of absorption, on all scales 10 – 10,000 km s⁻¹. On small scales the asymmetry comes from the density distribution in the low density IGM, making spectra that are largely absorption free, with occasional Ly α lines. On large scales the asymmetry comes from the rare high density regions that make absorption with large H I column densities. They make LLS and DLAs with strong Ly α lines, and they place many strong metal lines all across a spectrum.

15.3. Comparison with Hydrodynamic Simulations

We find that a hydrodynamic simulation on a 1024³ grid in a 75.7 Mpc box reproduces the observed mean DA from the IGM alone when we use popular parameters $H_0 = 71 \text{ km s}^{-1}\text{Mpc}^{-1}$, $\Omega_b = 0.044$, $\Omega_m = 0.23$ and $\Omega_\Lambda = 0.73$, $\sigma_8 = 0.9$ and a UV background with an ionization rate per H I atom of $\Gamma_{912} = (1.44 \pm 0.11) \times 10^{-12} \text{ s}^{-1}$ that is $\gamma_{912} = 1.08 \pm 0.08$ times the value calculated by Madau et al. (1999) with 61% from QSOs and 39% from stars. This value of the Γ is similar to the $\Gamma_{912} > 1.5 \times 10^{-12} \text{ s}^{-1}$ from Steidel et al. (2001) at $z \simeq 3$.

The mean DA that we measure for the Ly α from the low density IGM provides a joint constraint on two cosmological parameters, Ω_b and σ_8 , and one astrophysical parameter, Γ_{912} . Using $\Omega_b = 0.0444 \pm 0.0018$, $\sigma_8 = 0.9 \pm 0.1$ and $DA = 0.118 \pm 0.010$ we find $\Gamma_{912} = (1.44 \pm 0.36) \times 10^{-12} \text{ s}^{-1}$, where the error includes the contributions from the errors in Ω_b , σ_8 and DA, but not Ω_m or Ω_Λ .

The baryon density that accounts for the DA in the IGM at $z = 1.9$ is the same as the value measured using D/H and the CMB, with an uncertainty of about 6%. When we use $\sigma_8 = 0.9 \pm 0.1$, $\Gamma = 1.329 \pm 0.133 \times 10^{-12} \text{ s}^{-1}$ and $DA = 0.118 \pm 0.010$, we found $\Omega_b = 0.0417 \pm 0.0022$, where the error is from the DA alone (Table 5), or ± 0.0085 using the errors on all the listed parameters. This value agrees with the D/H + BBN value,

$\Omega_b = 0.042 \pm 0.004$ (Kirkman et al. 2003), and with the value from the first year WMAP data, $\Omega_b = 0.0444 \pm 0.0018$ (Spergel et al. 2003).

When we pass multiple lines of sight through the hydrodynamic simulation, we see slightly less variation in the DA in $\Delta z = 0.1$ than the Kast spectra IGM only, in part because of the box lacks large scale power. The power of the flux in these lines of sight does match that in HIRES spectra on scales $0.008 < \log k < 0.08$ (s/km).

15.4. Opportunities for Improvement

The values in Table 4 suggest that we could improve the accuracy of our mean DA4 measurement by observing many more QSOs, even without any improvements in the methods. The measurement error for the Kast spectra (column 4) would approach that from the S/N and continuum fits (column 3) with a sample about 4 times larger, or 300 QSOs. Here we assume that the DA4 values, each averaged over a path of 19.75, will be nearly normally distributed. The values given here are approximate, since they assume that the artificial spectra are an adequate representation of the IGM, even though they do not explicitly include absorption from high N_{HI} lines and metal lines.

We find that S/N = 6 per 1.13 Å in the observed frame is adequate for continuum placement in Kast spectra. With improved continuum placement methods we might be able to use lower S/N, but we would not be able to adjust the continua to fit the emission lines of each individual QSO, and hence the continuum fit errors will complicate the measurement of the large scale power.

High resolution spectrographs have the major advantage of allowing us to find and remove the individual Ly α lines of LLS and the metal lines in the Ly α forest. This reduces the sample size required for a given $\sigma(DA)$ by about a factor of four, and it greatly improves the accuracy of the corrections for the LLS and metal lines. The factor of four largely compensates for the lower efficiency of high resolution spectrographs in terms of photon recorded per Å per second. However, to find metal lines in high resolution spectra we would prefer S/N > 10 per 0.03 Å, which is about 100 times more photons per Å than we have with Kast spectra. We would also require improvement in the flux calibration and continuum fits to the high resolution spectra (Suzuki et al. 2003).

16. Acknowledgments

This work was funded in part by grant NAG5-13113 from NASA and by grant AST-0098731 from the NSF. The spectra were obtained from the Lick observatory and we thank the Lick Observatory staff. We are very grateful to Avery Meiksin and Rupert Croft for drawing our attention to this topic, and helping us understand the issues. We are especially grateful to Pat McDonald for providing us with the artificial absorption spectra and their description, and for many detailed comments on the manuscript. This research has made extensive use of the NASA/IPAC Extragalactic Database (NED) which is operated by JPL, under contract with NASA.

REFERENCES

- Abel, T. & Haehnelt, M. G. 1999, *ApJ*, 520, L13
- Bernardi, M., Sheth, R. K., SubbaRao, M., Richards, G. T., Burles, S., Connolly, A. J., Frieman, J., Nichol, R., Schaye, J., Schneider, D. P., Vanden Berk, D. E., York, D. G., Brinkmann, J., & Lamb, D. Q. 2003, *AJ*, 125, 32
- Bi, H. G., Boerner, G., & Chu, Y. 1992, *A&A*, 266, 1
- Bryan, G. L. & Machacek, M. 2000, *ApJ*, 534, 57
- Burles, S. 1997, Ph.D. Thesis (UCSD)
- Carswell, R. F., Whelan, J. A. J., Smith, M. G., Boksenberg, A., & Tytler, D. 1982, *MNRAS*, 198, 91
- Croft, R. A. C., Hernquist, L., Springel, V., Westover, M., & White, M. 2002a, *ApJ*, 580, 634
- Croft, R. A. C., Weinberg, D. H., Bolte, M., Burles, S., Hernquist, L., Katz, N., Kirkman, D., & Tytler, D. 2002b, *ApJ*, 581, 20
- Croft, R. A. C., Weinberg, D. H., Katz, N., & Hernquist, L. 1997, *ApJ*, 488, 532
- Fang, Y., Fan, X., Tytler, D., & Crofts, A. P. S. 1998, *ApJ*, 497, 67
- Gnedin, N. Y. & Hamilton, A. J. S. 2002, *MNRAS*, 334, 107
- Haardt, F. & Madau, P. 1996, *ApJ*, 461, 20
- Haehnelt, M. G., Madau, P., Kudritzki, R., & Haardt, F. 2001, *ApJ*, 549, L151
- Hu, E. M., Kim, T., Cowie, L. L., Songaila, A., & Rauch, M. 1995, *AJ*, 110, 1526
- Hui, L. & Gnedin, N. Y. 1997, *MNRAS*, 292, 27
- Hui, L., Haiman, Z., Zaldarriaga, M., & Alexander, T. 2002, *ApJ*, 564, 525
- Jenkins, E. B. & Ostriker, J. P. 1991, *ApJ*, 376, 33
- Kim, T. S., Carswell, R. F., Cristiani, S., D’Odorico, S., & Giallongo, E. 2002, *MNRAS*, 335, 555
- Kim, T.-S., Cristiani, S., & D’Odorico, S. 2001, *A&A*, 373, 757

- Kim, T.-S., Viel, M., Haehnelt, M. G., Carswell, R. F., & Cristiani, S. 2004, MNRAS, 347, 355
- Kirkman, D. & Tytler, D. 1997, ApJ, 484, 672
- Kirkman, D., Tytler, D., Suzuki, N., O’Meara, J. M., & Lubin, D. 2003, ApJS, 149, 1
- Kolb, E. W. & Turner, M. S. 1990, *The Early Universe* (Frontiers in Physics, Reading, MA: Addison-Wesley, 1988, 1990)
- Madau, P., Haardt, F., & Rees, M. J. 1999, ApJ, 514, 648
- McDonald, P. 2003, ApJ, 585, 34
- McDonald, P., Miralda-Escudé, J., Rauch, M., Sargent, W. L. W., Barlow, T. A., Cen, R., & Ostriker, J. P. 2000, ApJ, 543, 1
- Meiksin, A., Bryan, G., & Machacek, M. 2001, MNRAS, 327, 296
- Meiksin, A. & White, M. 2004, MNRAS, in press, astro-ph/0307289
- Misawa, T., Tytler, D., Iye, M., Storrie-Lombardi, L. J., Suzuki, N., & Wolfe, A. M. 2002, AJ, 123, 1847
- Norman, M. L. & Bryan, G. L. 1999, in *ASSL Vol. 240: Numerical Astrophysics*, 19
- Oke, J. B. & Korycansky, D. G. 1982, ApJ, 255, 11
- Peterson, B. A. 1978, in *IAU Symp. 79: Large Scale Structures in the Universe*, 389–392
- Press, W., Rybicki, G., & Schneider, D. 1993, ApJ, 414, 64
- Rauch, M. 1998, ARA&A, 36, 267
- Rauch, M., Miralda-Escude, J., Sargent, W. L. W., Barlow, T. A., Weinberg, D. H., Hernquist, L., Katz, N., Cen, R., & Ostriker, J. P. 1997, ApJ, 489, 7
- Sargent, W., Young, P., Boksenberg, A., & Tytler, D. 1980, ApJS, 42, 41
- Sargent, W. L. W., Steidel, C. C., & Boksenberg, A. 1988, ApJS, 68, 539
- Schachter, J. 1991, PASP, 103, 457
- Schaye, J., Aguirre, A., Kim, T.-S., Theuns, T., Rauch, M., & Sargent, W. L. W. 2003, ApJ, 596, 768

- Seljak, U., McDonald, P., & Makarov, A. 2003, MNRAS, 342, L79
- Spergel, D. N., Verde, L., Peiris, H. V., Komatsu, E., Nolta, M. R., Bennett, C. L., Halpern, M., Hinshaw, G., Jarosik, N., Kogut, A., Limon, M., Meyer, S. S., Page, L., Tucker, G. S., Weiland, J. L., Wollack, E., & Wright, E. L. 2003, ApJS, 148, 175
- Steidel, C. C. 1990, ApJS, 72, 1
- Steidel, C. C., Pettini, M., & Adelberger, K. L. 2001, ApJ, 546, 665
- Steidel, C. C. & Sargent, W. L. W. 1987, ApJ, 313, 171
- Stengler-Larrea, E. A., Boksenberg, A., Steidel, C. C., Sargent, W. L. W., Bahcall, J. N., Bergeron, J., Hartig, G. F., Jannuzi, B. T., Kirhakos, S., Savage, B. D., Schneider, D. P., Turnshek, D. A., & Weymann, R. J. 1995, ApJ, 444, 64
- Storrie-Lombardi, L. J. & Wolfe, A. M. 2000, ApJ, 543, 552
- Suzuki, N., Tytler, D., Kirkman, D., O’Meara, J. M., & Lubin, D. 2003, PASP, 115, 1050
- . 2004a, ApJ *in press*
- Telfer, R. C., Zheng, W., Kriss, G. A., & Davidsen, A. F. 2002, ApJ, 565, 773
- Tytler, D. 1982, Nature, 298, 427
- . 1987, ApJ, 321, 69
- Vanden Berk, D. E., Richards, G. T., Bauer, A., Strauss, M. A., Schneider, D. P., Heckman, T. M., York, D. G., Hall, P. B., Fan, X., Knapp, G. R., Anderson, S. F., Annis, J., Bahcall, N. A., Bernardi, M., Briggs, J. W., Brinkmann, J., Brunner, R., Burles, S., Carey, L., Castander, F. J., Connolly, A. J., Crocker, J. H., Csabai, I. ., Doi, M., Finkbeiner, D., Friedman, S., Frieman, J. A., Fukugita, M., Gunn, J. E., Hennessy, G. S., Ivezić, Ž., Kent, S., Kunszt, P. Z., Lamb, D. Q., Leger, R. F., Long, D. C., Loveday, J., Lupton, R. H., Meiksin, A., Merelli, A., Munn, J. A., Newberg, H. J., Newcomb, M., Nichol, R. C., Owen, R., Pier, J. R., Pope, A., Rockosi, C. M., Schlegel, D. J., Siegmund, W. A., Smee, S., Snir, Y., Stoughton, C., Stubbs, C., SubbaRao, M., Szalay, A. S., Szokoly, G. P., Tremonti, C., Uomoto, A., Waddell, P., Yanny, B., & Zheng, W. 2001, AJ, 122, 549
- Weinberg, D. H., Miralda-Escude, J., Hernquist, L., & Katz, N. 1997, ApJ, 490, 564
- Wolfe, A. M., Turnshek, D. A., Smith, H. E., & Cohen, R. D. 1986, ApJS, 61, 249

Zaldarriaga, M., Scoccimarro, R., & Hui, L. 2003, ApJ, 590, 1

Zhang, Y., Meiksin, A., Anninos, P., & Norman, M. L. 1998, ApJ, 495, 63

Zheng, W., Kriss, G. A., Telfer, R. C., Grimes, J. P., & Davidsen, A. F. 1997, ApJ, 475, 469

Table 1. DA as a Function of Redshift

z	Mean DA	$\sigma(\mu)$	15.8% below	15.8% above
1.64	0.1124	0.0089	-0.1303	0.3410
1.72	0.1359	0.0041	-0.0436	0.3160
1.80	0.1333	0.0034	-0.0143	0.2910
1.88	0.1398	0.0028	0.0015	0.2955
1.96	0.1681	0.0030	0.0071	0.3492
2.04	0.1714	0.0033	0.0114	0.3526
2.12	0.1973	0.0047	0.0168	0.4018
2.20	0.1775	0.0052	0.0185	0.3570
2.28	0.1667	0.0113	0.0001	0.3522
2.36	0.1576	0.0332	-0.0874	0.4461

Table 2. Absorption by Metal Lines

Parameter	λ_r (Å)	λ_{obs} (Å)	σ (%)	Mean (%)	$\sigma(Mean)$ (%)
DM1	1362	1.58	0.13
DM2	...	4158	...	1.58	0.13
DM3	1360	4135	2.5	1.87	0.13
DM4 SBS	1358	4125	2.7	1.67	0.22
DM5 SBS	1360	1.66	0.22
DM6 SBS	...	4158	...	1.65	0.22
DM7(CIV)	...	4580	...	0.69	0.15
DM7(CIV)	1360	0.71	...
DM7(CIV)	1120	0.80	...
DM1-6	1120	1.92	0.42
DMs	1120	2.3	0.5

Table 3. Distribution of the DA2s at $z = 1.9$ in $\Delta z = 0.1$ Segments

Data Set	Metals?	LLS?	n	$\sigma(\text{DA2})$	$\sigma[\sigma(\text{DA2})]$	Mean DA2	$\sigma\mu$
Kast Spectra	yes	yes	152	0.0612	0.0035	0.1563	0.0050
Kast < 0.35	yes	yes	151	0.0487	0.0028	0.1488	0.0049
Ly- α of LLS	no	yes	471:	0.0351	0.0047	0.0103	0.004
Metals (DM3, DMs)	yes	no	377	0.031	...	0.023	0.005
$\sigma(\Delta z = 0.1)$ Kast IGM only	no	no	152	0.039	$^{+0.005}_{-0.007}$	0.118	0.010
Artificial Spectra	no	no	150	0.0422	0.0024	0.1518	0.0035
Hydro. Spectra	no	no	150	0.0331	0.0019	0.1287	0.0027

Table 4. DA3s Values for Quarters of the Kast and Artificial Spectra

	Artificial True	Artificial Measured	Artificial True - Measured	Kast Measured	Mean z_{abs}
First Quarter	0.1574	0.1577	-0.00027	0.1487	1.949
Second Quarter	0.1668	0.1660	0.00075	0.1456	1.936
Third Quarter	0.1433	0.1486	-0.00531	0.1696	1.966
Fourth Quarter	0.1546	0.1449	0.00990	0.1404	1.846
σ	0.0097	0.0095	0.00634	0.0128	...
Mean μ	0.1555	0.1543	0.00127	0.1511	1.924
$\sigma(\mu)$	0.0048	0.0048	0.00317	0.0064	...

Table 5. DA8s for Various combinations of Cosmological Parameters

Parameter measured	Ω_b	σ_8	γ_{912}	γ_{228}	DA8s
all	0.0444 ± 0.0018	0.9 ± 0.1	1.0 ± 0.1	1.8	0.118 ± 0.010
DA in sim.	0.0440	0.9	1.0	1.8	0.1287 ± 0.0027
γ_{912}	0.0440	0.9	1.08 ± 0.08	1.8	0.118
σ_8	0.0440	0.94 ± 0.04	1.0	1.8	0.118
Ω_b	0.0417 ± 0.0022	0.9	1.0	1.8	0.118
γ_{912}	0.0444 ± 0.0018	0.9 ± 0.1	1.08 ± 0.27	1.8	0.118 ± 0.010

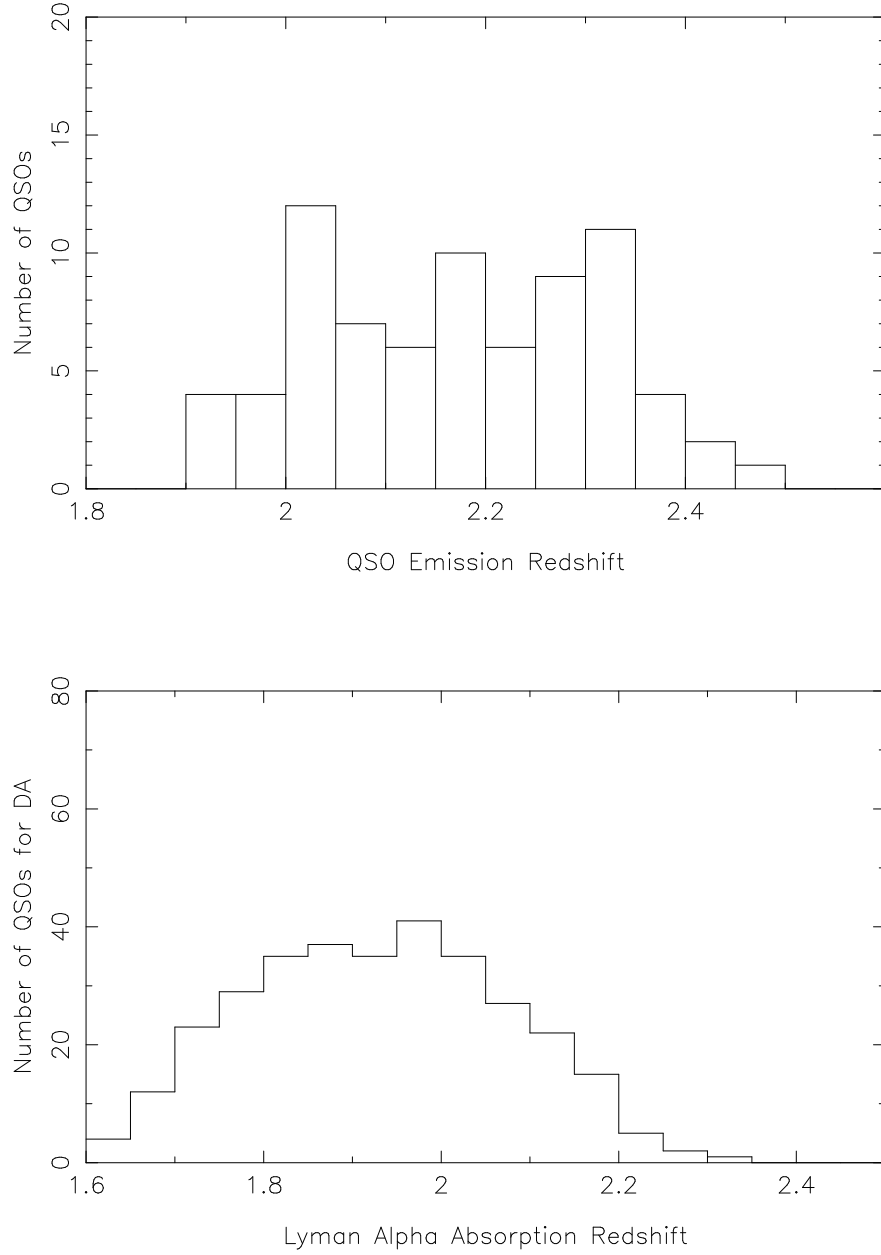


Fig. 1.— **Top panel:** The number of QSOs in our sample as a function of emission redshift. **Bottom panel:** The number of QSOs which contribute to our measurement of DA at each redshift.

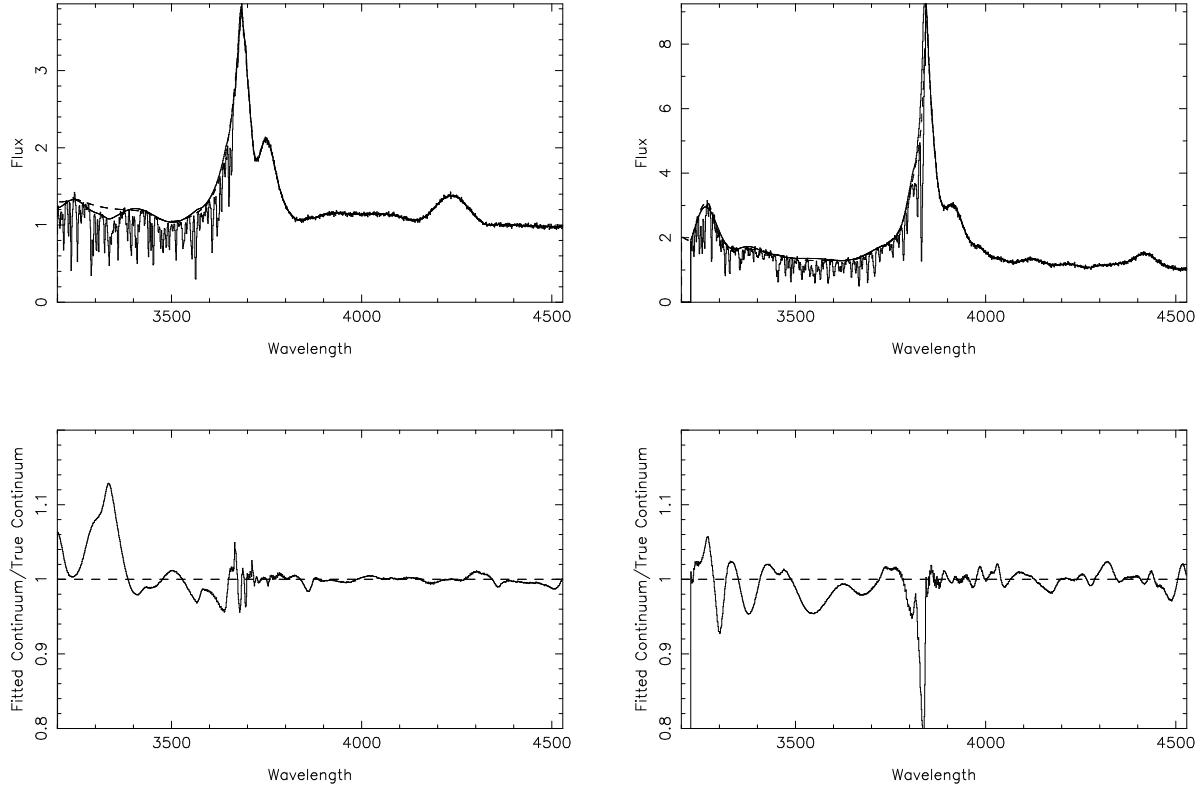


Fig. 2.— Examples of the continua that we fit to two artificial QSO spectra. In the top panel for each QSO the solid curve is the true continuum and the dashed line our fit. Under each spectrum we show the fitted continuum divided by the true continuum: $F1/TC$. The spectrum on the left has the largest error in the Ly α forest of any spectrum with high S/N. The artificial spectrum on the right was selected at random, and also happens to have high S/N.

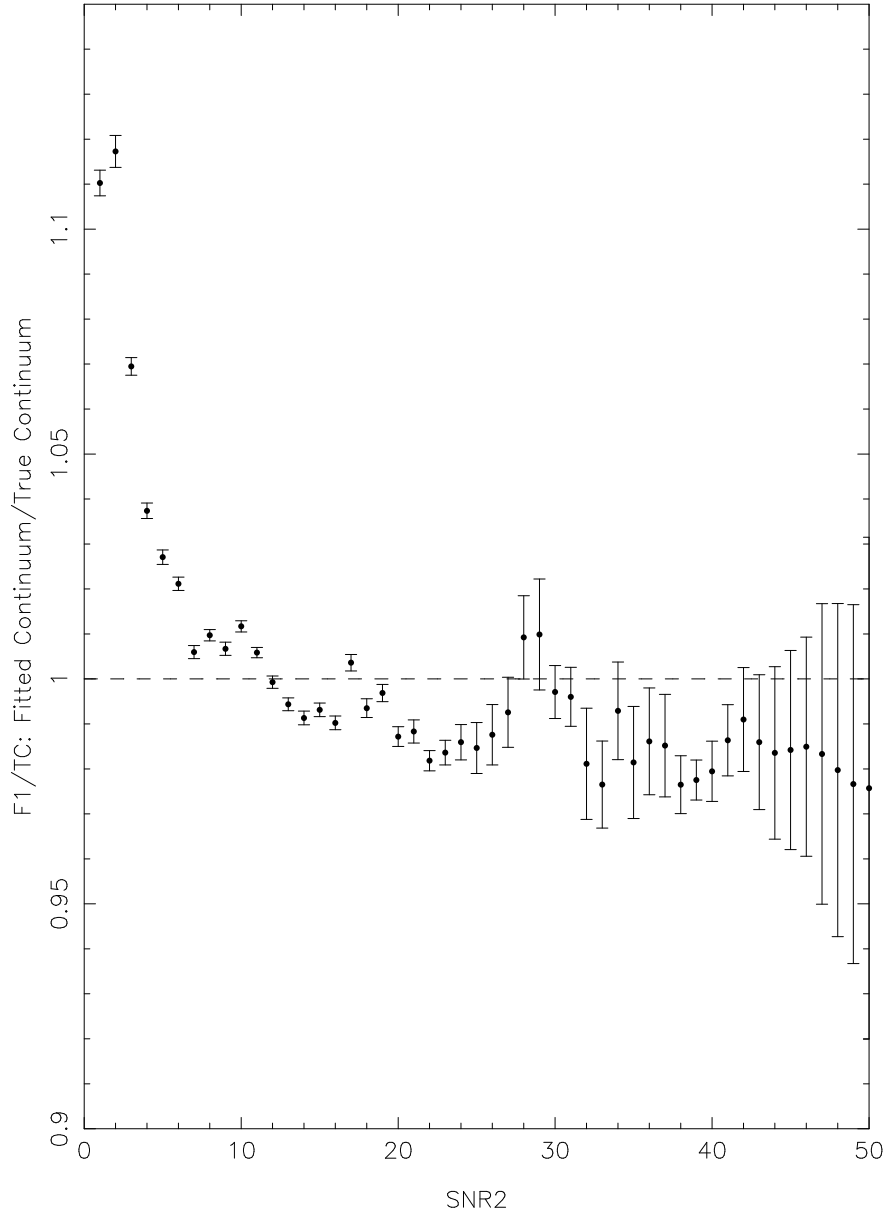


Fig. 3.— The fractional error in the continuum level as a function of the data quality. The points show the ratio of our fitted continuum to the true continuum, $F1/TC$, in the artificial QSOs as a function of $SNR2$. The error bars on each point indicate the error on the mean value of the fitted/true continuum ratio. The $F1/TC$ values for each pixel have a much larger dispersion, especially for small $SNR2$.

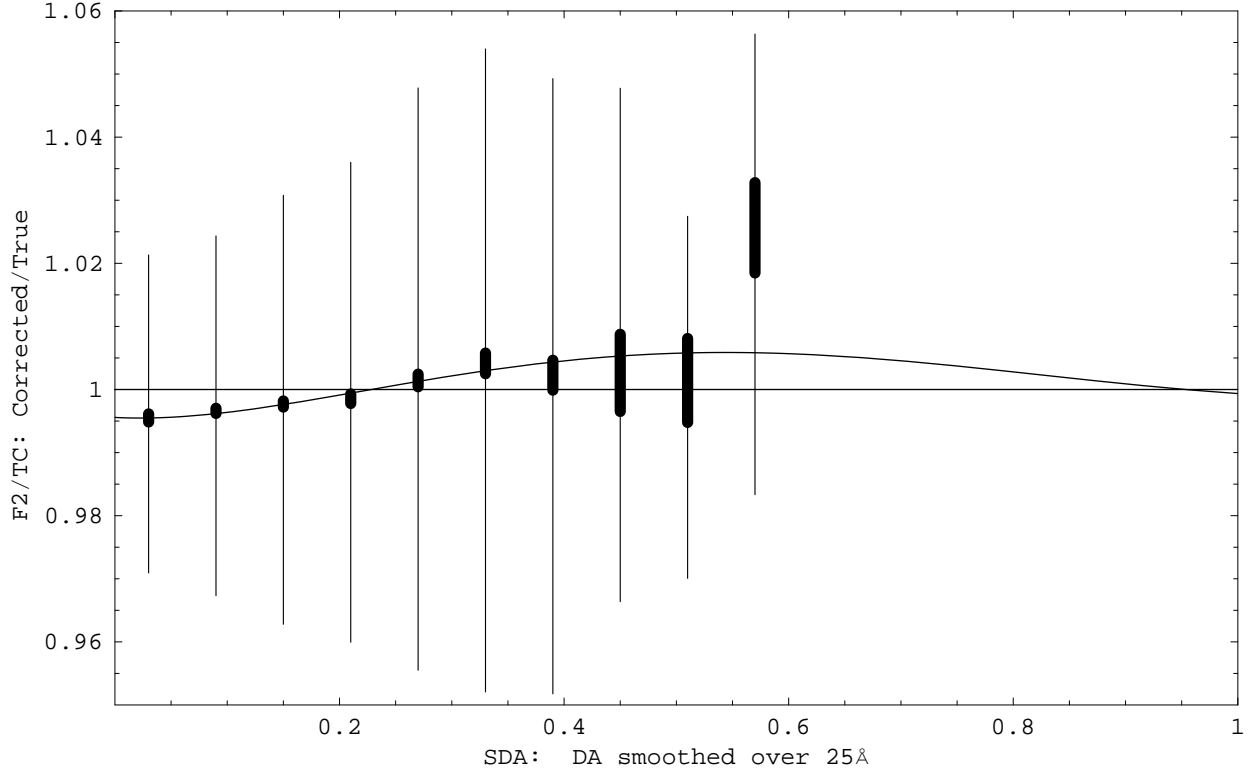


Fig. 4.— Fractional error in the partly corrected continuum level as a function of the mean amount of absorption. The points show the ratio of the continuum corrected for the SNR2 correlation to the true continuum in the artificial QSO spectra, $F2/TC$, as a function of SDA. The thick bars indicate the mean and the error on the mean at each SDA value. The thin bars show $\pm 1\sigma$ for the $F2/TC$ evaluated in all pixels in the SDA interval. The smooth curve is the function we used to implement the SDA correction.

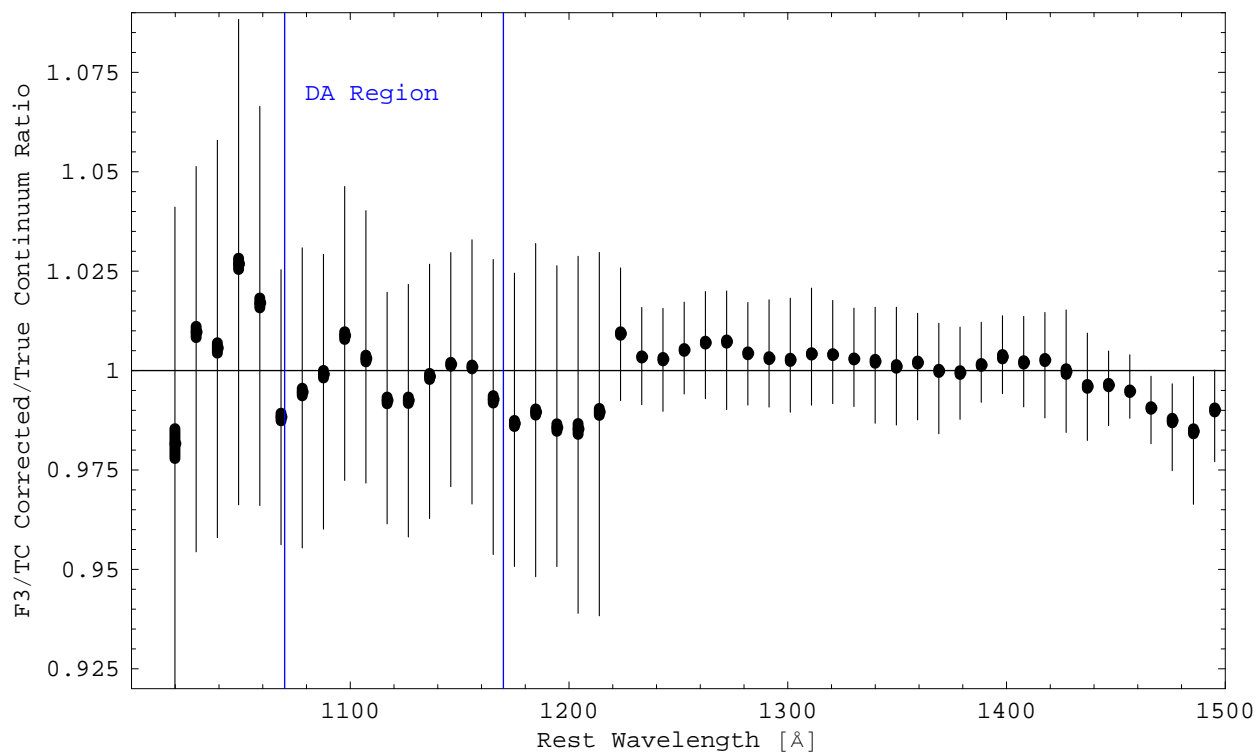


Fig. 5.— Fractional error in the fully corrected continuum level as a function of rest wavelength. We show the ratio of our F3 continuum to the true continuum in our sample of artificial spectra. The F3 continuum has our SNR2 and SDA corrections applied for $\lambda_r < 1216$ Å, while for higher wavelengths the F3 continuum is the original F1 continuum. The two vertical lines show 1070 and 1170 Å, the boundaries of the region where we measure DA.

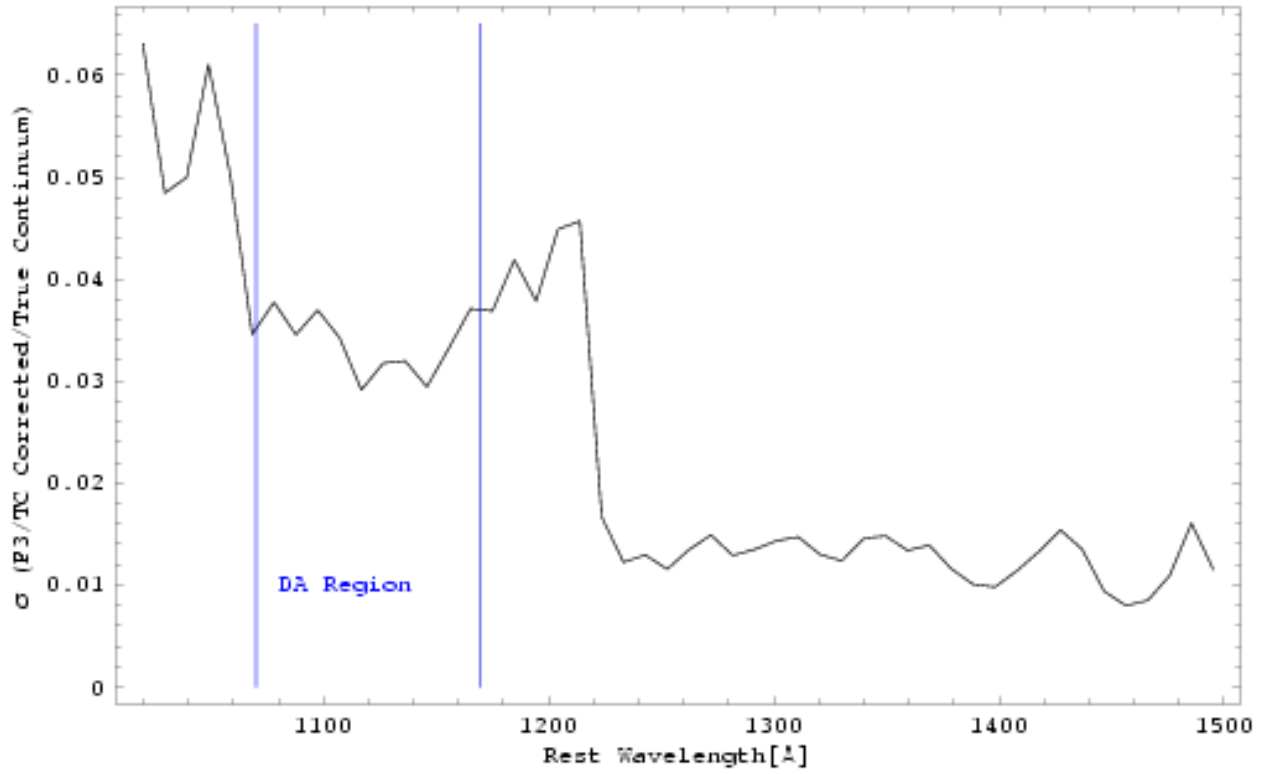


Fig. 6.— The standard deviation of the fractional error in our continuum fits to the artificial spectra, F3/TC. Our continuum fits appear to be well behaved in the region we use to measure DA: $1070 < \lambda_r < 1170 \text{ \AA}$.

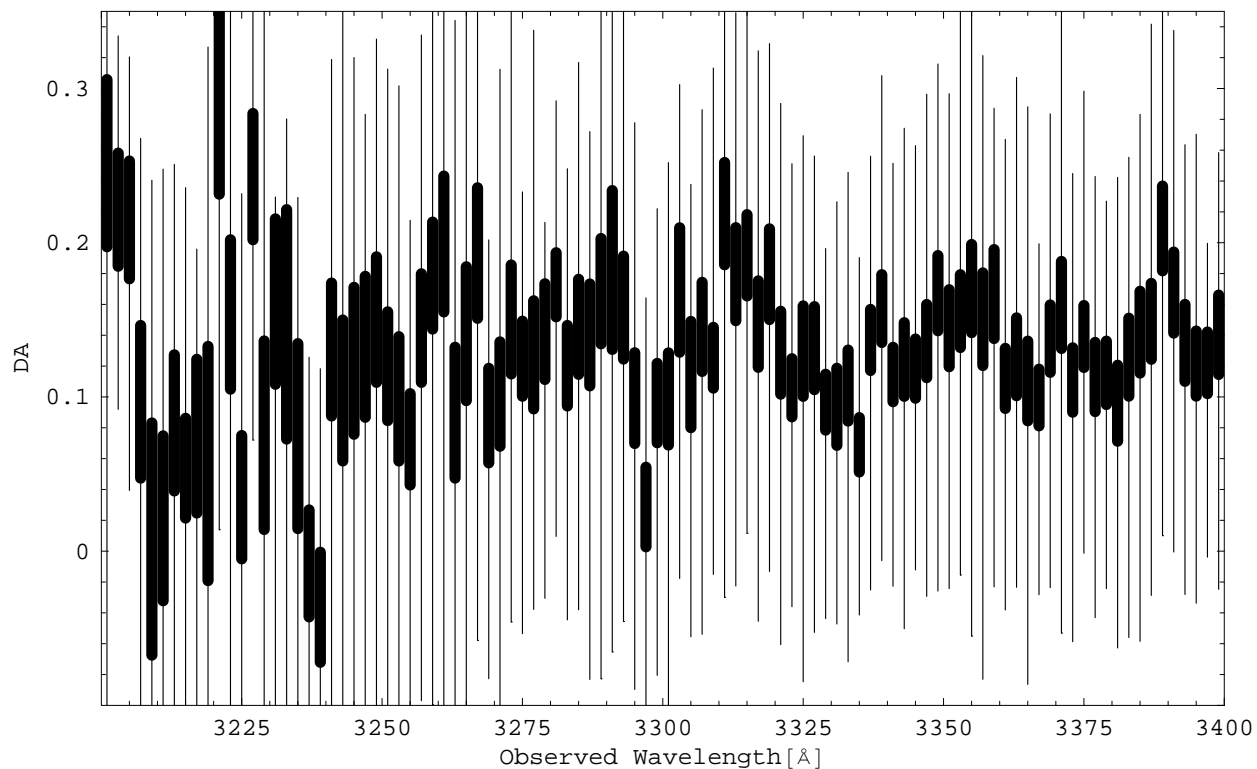


Fig. 7.— The total amount of absorption, shown as DA, in the Kast spectra as a function of observed wavelength where Ozone absorption is expected. We expect the most Ozone absorption, and the highest DA values, near the marked wavelengths, 3198, 3220, 3252, 3280 and 3310 Å. As in previous Figures, the center of each thick bar is at the mean DA value in the bin, and its length is the $\pm 1\sigma$ error on the mean, while the thin lines the $\pm 1\sigma$ of the DA values per pixel.

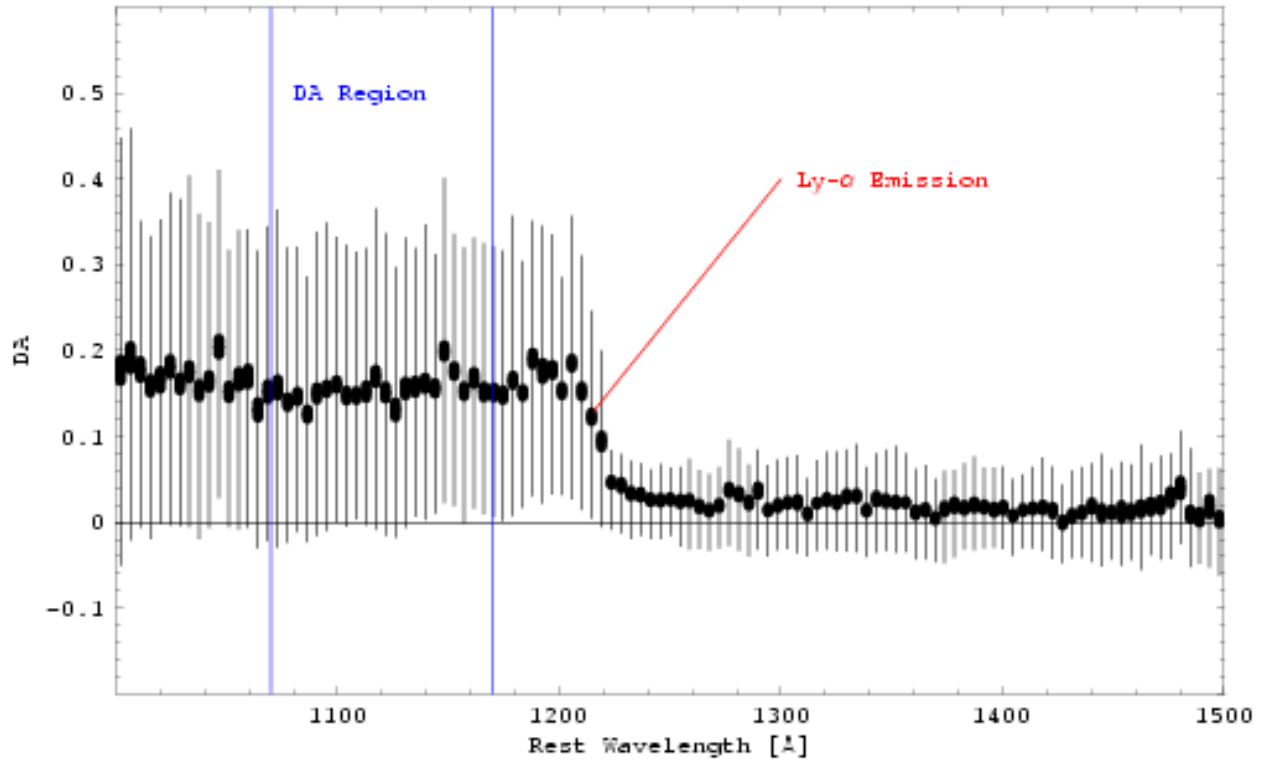


Fig. 8.— Total absorption in the Kast spectra, shown as DA, as a function of rest wavelength. The DA includes absorption by Ly α in the IGM, in LLS, DLAs and metal lines. The thin lines show the $\pm 1\sigma$ values for the DA0 per pixel. The heavy lines show the mean and error on the mean DA in the 4.5 Å bins, the DA1 values.

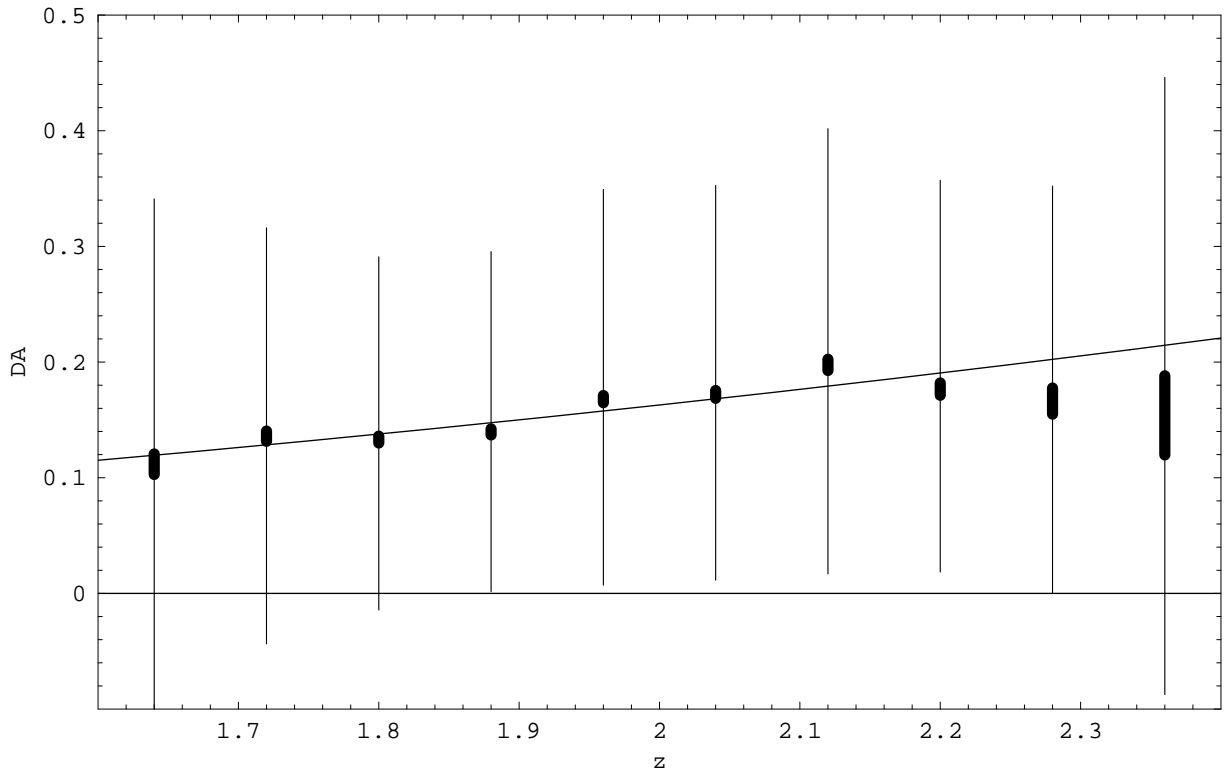


Fig. 9.— The total amount of absorption in the Kast spectra from rest wavelengths 1070 – 1170 Å as a function of Ly α redshift. We show the mean DA values for all pixels with z_{abs} in the indicated ranges. The measurements from each QSO contribute to 1 – 3 bins. The DA values include contributions from the Ly α in the IGM, in LLS, DLAs and metal lines. The errors are as in similar Figures.

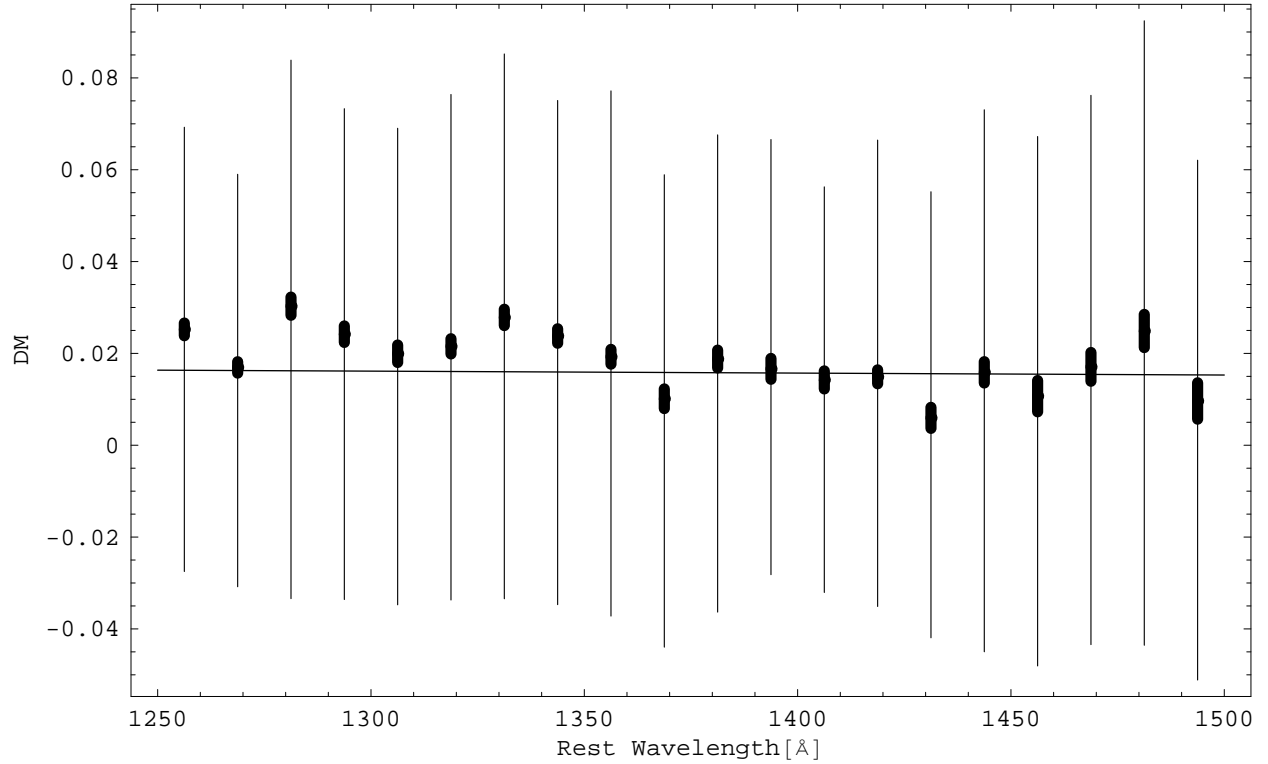


Fig. 10.— The amount of absorption in the Kast spectra from metal lines, DM, as a function of rest wavelengths. For our convenience, in this plot, we use DM values that we calculated using the raw fitted continua, without correction for the correlations with SDA or SNR2. Because of this, the points are too high by an average of 0.495% and the mean value on the plot is 2.36%, instead of the correct value of 1.87%. Values can be negative because of photon noise and continuum fitting errors. The line is the DM1 fit.

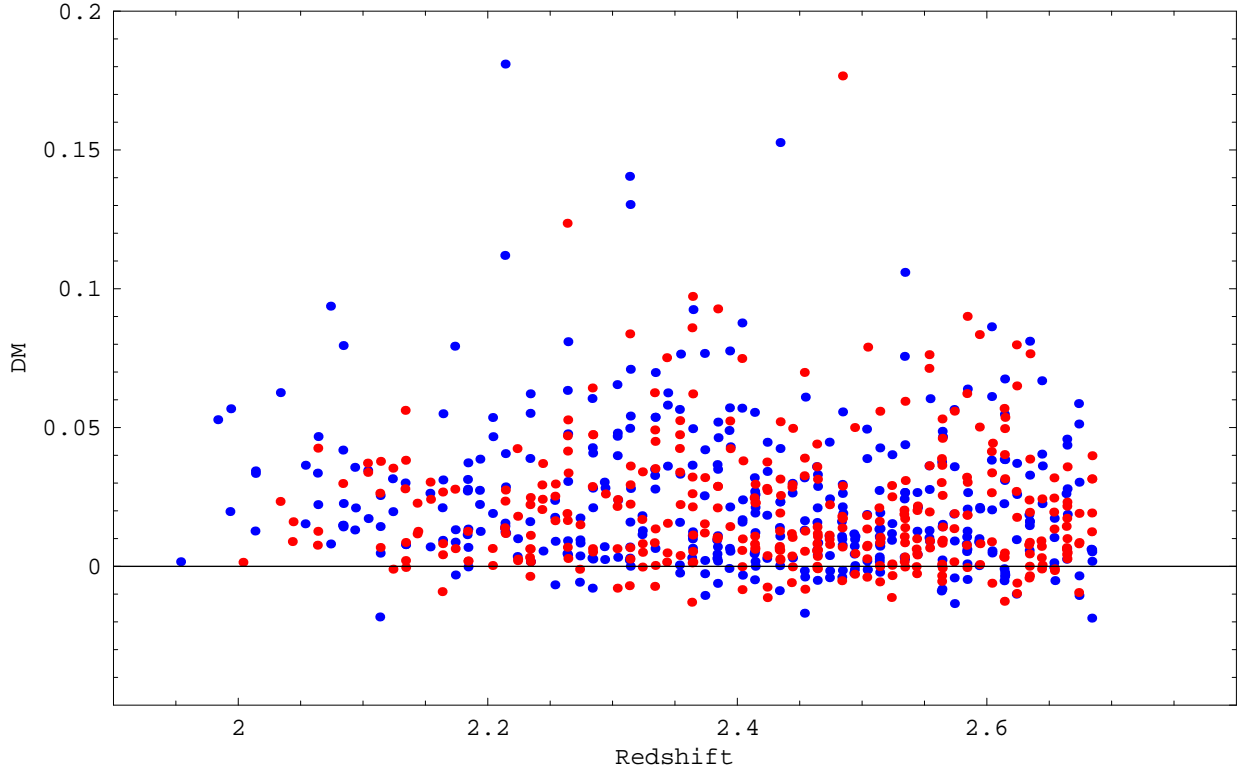


Fig. 11.— The amount of absorption by metal lines in the Kast spectra, DM2 values, as a function of redshift z for Ly α . Observed wavelength is $1215.67 \times (1 + z)$. The 377×2 DM2 values are the mean values, in adjacent segments of spectrum 121.567 \AA long. The lighter points (red) are from bins shifted from the darker (blue) ones by $\Delta z = 0.05$, one half the bin size of both points, hence most portions of a given spectrum contribute to two points. For our convenience, in this plot, we use DM2 values that we calculated using the raw fitted continua, without correction for the correlations with SDA or SNR2. Because of this, the points are too high by an average of 0.495% and the mean value on the plot is 2.36% , instead of the correct value of 1.87% . Values can be negative because of photon noise and continuum fitting errors.

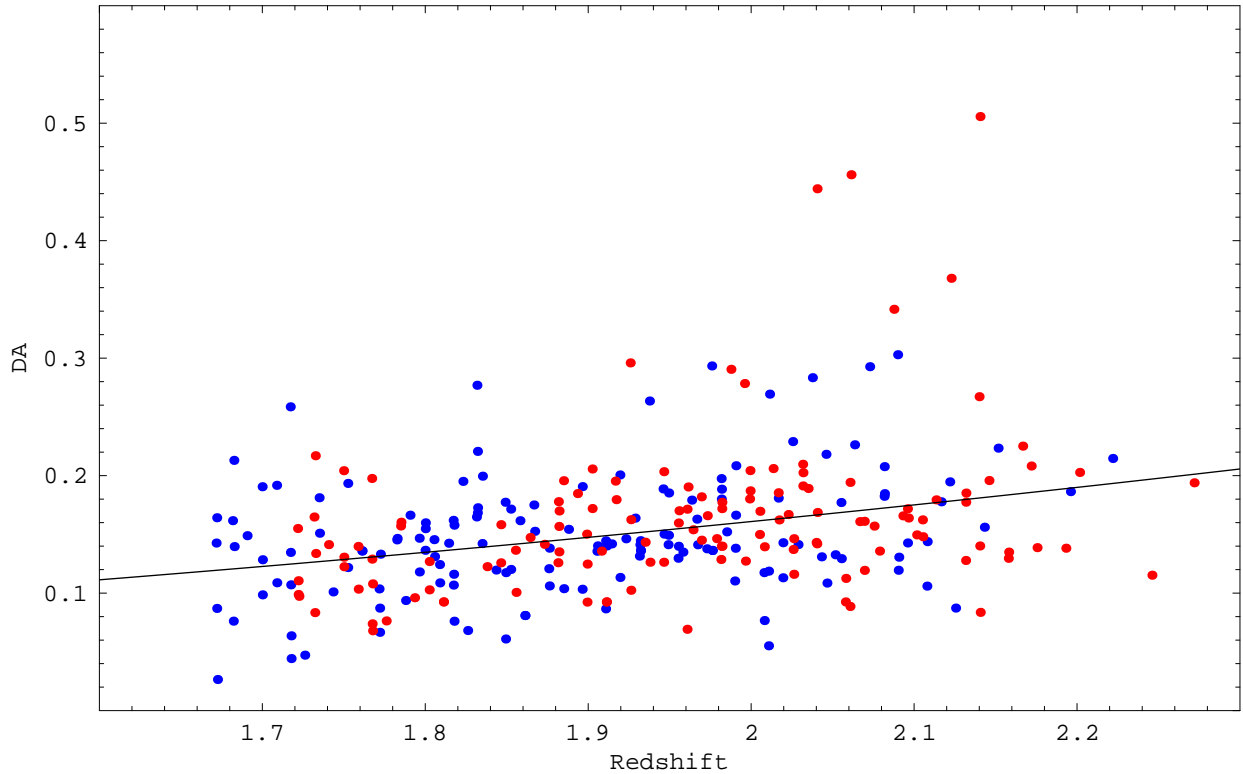


Fig. 12.— The total amount of absorption in the Kast spectra in the rest frame interval $1070 - 1170 \text{ \AA}$ as a function of redshift of Ly α . The absorption includes Ly α from the IGM, LLS, DLAs and metal lines. The points are DA2 values, the means in segments of length $\Delta z = 0.1$ or 121.567 \AA in the observed frame. The solid line indicates the fit to the redshift evolution of DA, given by Equation (4). The lighter points (red) are from bins shifted from the darker (blue) ones by $\Delta z = 0.05$, one half the bin size of both points. Most of the largest values come from DLAs, some of which are split between two adjacent bins.

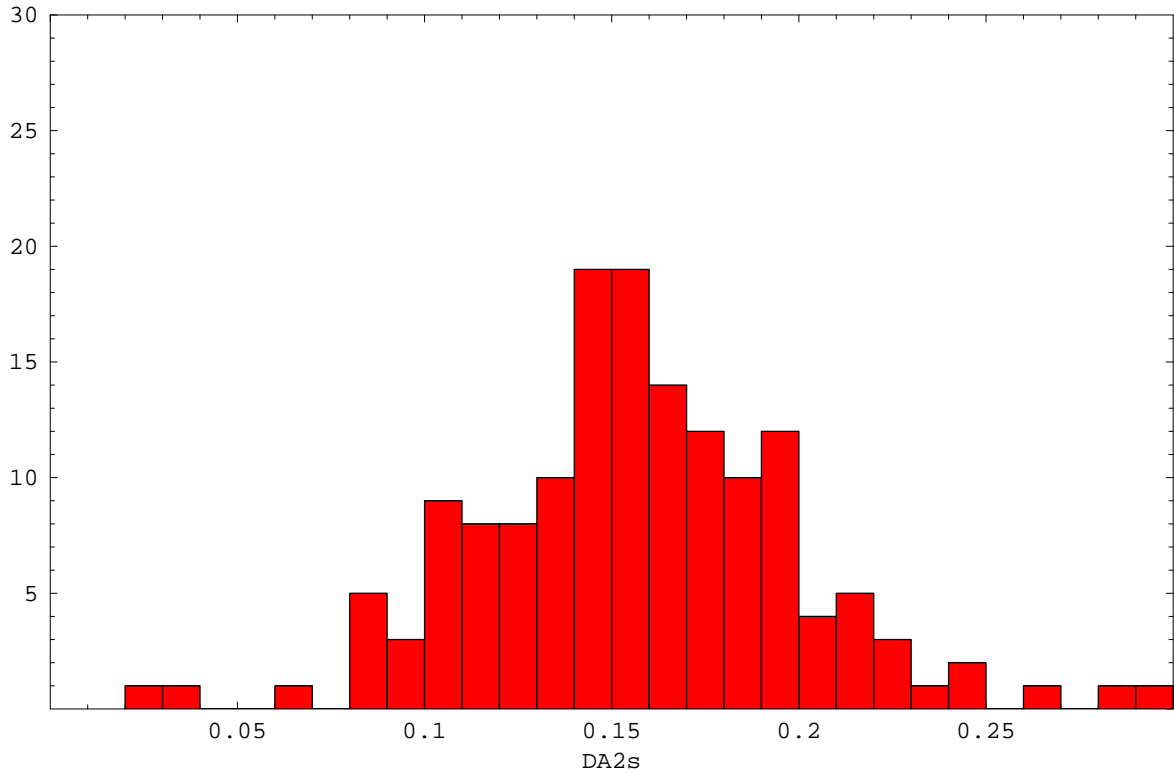


Fig. 13.— The distribution of DA2s values from the Kast spectra. These are the mean DA values in bins of size $\Delta z = 0.1$. The values have been scaled, pixel by pixel, to the DA expected at $z = 1.9$ using the trend of Equation (4). These DA values include absorption by metal lines and the Ly α lines from the IGM, LLS and DLAs. Each portion of a spectrum contributes to a maximum of one value to this histogram. Unlike Figure 12 we do not use bins shifted by 0.05 in z . One DA2s value is too large to appear on the plot.

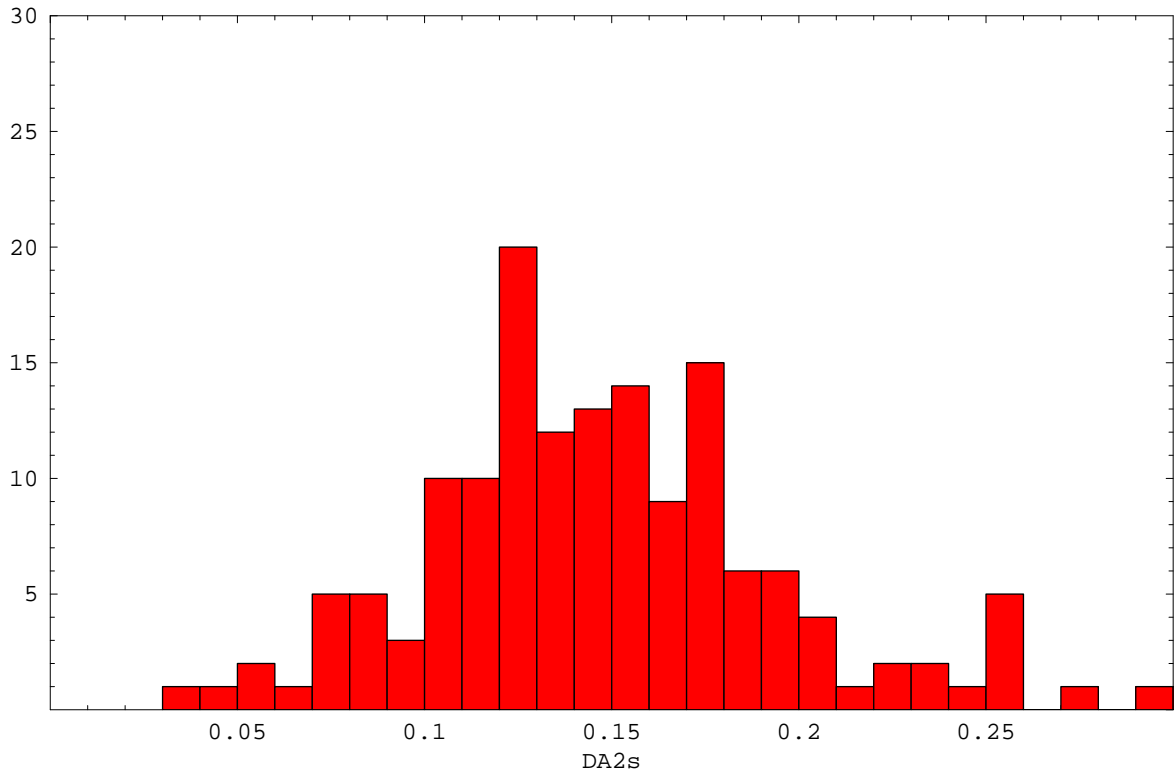


Fig. 14.— As Figure 13, but for the artificial spectra that we used to determine the corrections we applied to our continuum levels. All the DA2s values are shown.

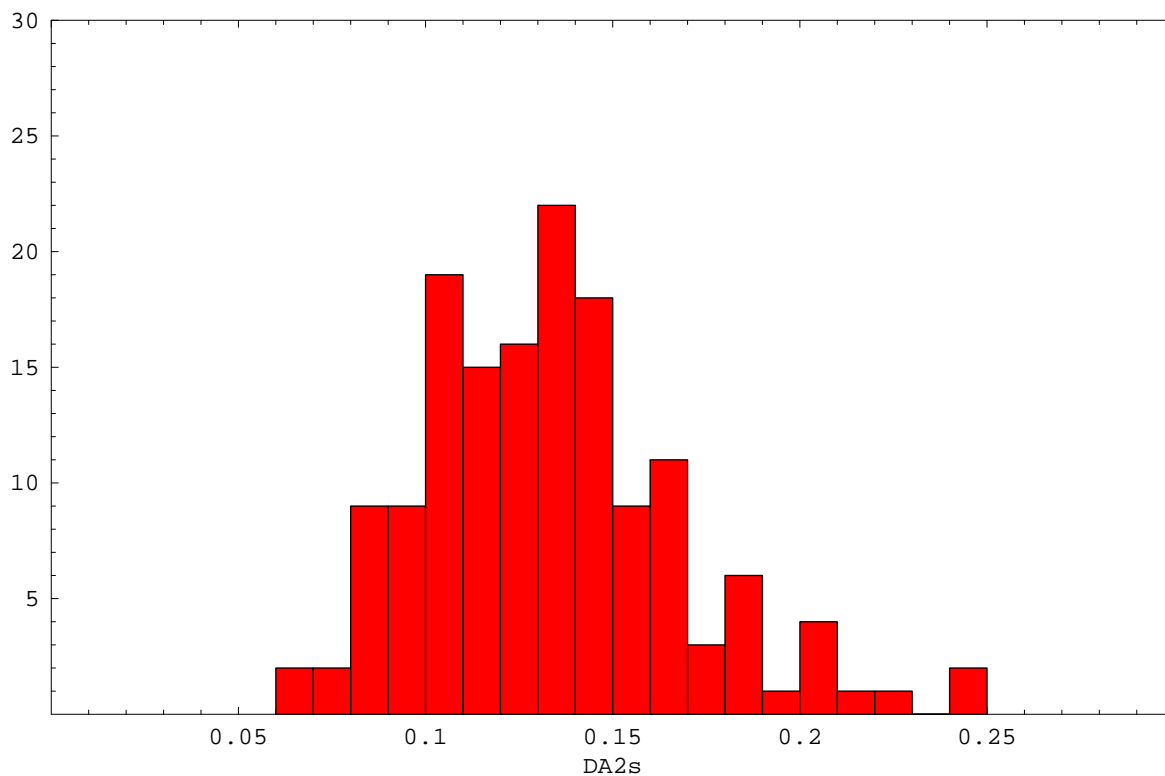


Fig. 15.— As Figure 13, but showing DA2 values for spectra from a full hydrodynamic simulation of the IGM, in a 75.7 Mpc with a grid size of 1024^3 . The simulation does not include $\text{Ly}\alpha$ from LLS and DLAs, and it does not include metal absorption. The bins were taken between $1.9 < z < 2.0$, and the simulation evolved slightly in this interval. We did not scale these DA2 values to $z = 1.9$.

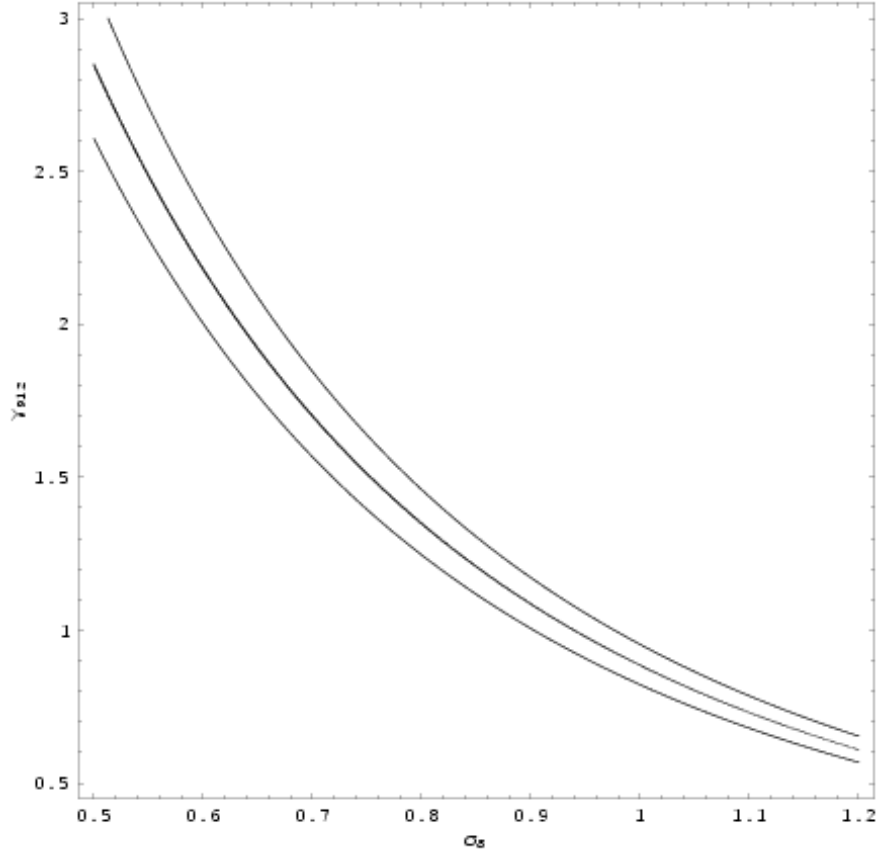


Fig. 16.— The ionization rate per H I atom in the IGM as a function of the amplitude of the matter power spectrum σ_8 . The vertical axis is the ionization rate per H I atom, Γ , in units of that given by Madau et al. (1999). When we adopt their spectrum Γ is proportional to the intensity of the radiation intensity J_{912} . The central curve shows the approximate Γ and σ_8 values that give the $DA8s = 0.118 \pm 0.010$ that we measured in the Kast spectra for the low density IGM only, at $z = 1.9$. The outer two curves give the $\pm 1\sigma$ range for the DA8s. These DA values exclude metal lines and the Ly α lines of LLS. Models with larger Γ , and larger σ_8 than the curves, in the upper right, have too little absorption, while those below have too much. Larger Γ values leave less H I and less absorption than we see. Larger σ_8 leaves fewer baryons in the IGM where we get the most absorption per baryon.